

Simple Book Example

TeXstudio Team

January 2013

ii

thesis

Contents

1	Theory and methods of plenoptic imaging	1
1.1	Introduction	1
1.2	Plenoptic function and the light field	3
1.3	Plenoptic camera	6
1.4	Optical Phase Space	9
1.5	Plenoptic 1.0	10
1.5.1	Phase space in plenoptic 1.0	14
1.5.2	Light Field Parametrization	16
1.6	Plenoptic 1.0 rendering	21
1.6.1	Changing Aperture and point of view	24
1.7	Synthetic refocus	26
1.8	Depth estimation	26
2	Fresnel Simulation Toolbox	27
2.1	Introduction	27
2.2	Scalar Theory of diffraction	28
2.2.1	Helmotz equation	31
2.2.2	Solutions of Helmholtz Equations	32
2.2.3	The Fresnel Approximation	33
2.3	Operator Free space propagation: Fresnel Approximation approach	34
2.3.1	Multi-Step Fresnel propagation operator	36
2.4	Operator Free space propagation: Angular spectrum of plane waves approach	38
2.4.1	Angular spectrum of plane waves	38
2.4.2	Band Limited Angular Spectrum	42
2.4.3	Corrected Band Limited Angular Spectrum Method	46
2.5	Operator Thin Lens	52
2.5.1	Aliasing in phase sampling	56
2.6	Comparison between the free space propagation operators	58
2.6.1	Description of the system	59

2.6.2	Image of a point source	60
2.6.3	Frequency analysis	62
2.7	Coherence	65
2.7.1	Temporal coherence	66
2.7.2	Spatial Coherence	67
2.7.3	Simulation of spatial coherence	67
2.7.4	Simulation of temporal coherence	72
2.8	Optimization of coherence parameters	74
2.8.1	Optimization of Spatial Coherence	74
2.8.2	Optimization of temporal coherence	78
2.8.3	Coherent imaging vs incoherent imaging	80
3	Simulations of a plenoptic 1.0 system	83
3.1	Description of the system	83
3.2	Computer generated light fields	83
3.3	Rendering	83
3.4	Depth estimation	83
3.5	Tomography	83
3.6	Conclusion	83
4	Simulation of a plenoptic 2.0 system	85
4.1	Description of the system	85
4.2	Optical performances of a focused plenoptic system	85
4.3	Optical resolution	85
4.3.1	Impulse response ans OTF	85
4.3.2	Two point resolution	85
4.3.3	Optical cutoff frequency	85
4.4	Aberrations	85
5	Light Field Microscope	87
5.1	Introduction	87
5.2	optical setup	87
5.3	Performances of the system	87

List of Figures

1.1	Differences between a traditional camera and a computational camera [10].	2
1.2	Two point representation of light field. Each ray of light if unequivocally defined by the coordinates of two point of interception.	5
1.3	Point angle representation. A ray of light is unequivocally defined by the coordinates of a point that belongs to a plane perpendicular at the optical axis z and by the angles θ_x and θ_y that it forms with the optical axis along the directions x and y.	5
1.4	Plenoptic camera and its fundamental components. The presence of the micro array allows to record the light field	7
1.5	Top: Plenoptic camera 1.0. The main lens is focused at infinity, forms an image on the micro array and the micro array are focused on the sensor. f is the focal length of the main lens and f_μ the focal length of the micro lens array. Bottom: Plenoptic camera 2.0. The main lens is focused at infinity and forms an image on the plane represented by the dashed line. The micro array acts as a relay between the main lens image and the sensor, since it satisfies the lens equation $1/a+1/b = 1/f_\mu$	8
1.6	The optical momentum correspond to the direction of the ray of light.	9
1.7	Ray diagram of a plenoptic 1.0 system. The main lens is in a 2f configuration respect the micro array. The sensor plane is conjugated with the main lens plane. The micro lens position maps the position (x,y) of the point P, while the sub image maps the directions of the rays coming from that point. The ray with direction θ_1 falls on the pixel 1 (blue), the ray with direction θ_2 falls on the pixel 2 (green) and the ray with direction θ_3 falls on the pixel 3 (red). The sub image d maps the direction of the ray.	11

1.8 Ray diagram of a plenoptic 1.0 system. The main lens is in a 2f configuration respect the micro array. The sensor plane is conjugated with the main lens plane. The micro lens position maps the position (x,y) of the point P, while the sub image maps the directions of the rays coming from that point. The ray with direction θ_1 falls on the pixel 1 (blue), the ray with direction θ_2 falls on the pixel 2 (green) and the ray with direction θ_3 falls on the pixel 3 (red). The sub image d maps the direction of the ray.	13
1.9 F-number matching between the main lens and the micro lens in the array.	14
1.10 Sampling of the light field and phase space representations of the rays.	15
1.11 Example of a raw plenoptic 1.0 image.	17
1.12 Zoom on the raw image. Each lenslet is formed by 20 by 20 pixel. each pixel represent a direction of the rays hitting the lens let that produced the sub image.	17
1.13 The array view is an array of the different point of view obtained rearranging the pixel according to the directional coordinates.	18
1.14 The array view is an array of the different point of view obtained rearranging the pixel according to the directional coordinates.	19
1.15 Zoom of the central part of the array view showing in detail the different point of views	20
1.16 Sampling of the light field and phase space representations of the rays.[11]	21
1.17 Rendering seen from the (x, θ_x) slice of the phase space. [5] . .	23
1.18 rendered image form the raw data in figure 1.11. Resolution is only 75 by 75 pixel. [5]	24
1.19 Rendering seen from the (x, θ_x) slice of the phase space. In grey are shown the directional pixels not considered for the integration.	25
1.20 Rendering seen from the (x, θ_x) slice of the phase space. In grey are shown the directional pixels not considered for the integration.	25
2.1 example	33

2.2	To remove the scaling factor between the input and output fields, we developed a multi step Fresnel approach. The field is propagated by unit of dz , the minimum distance to keep the sampling the same.	36
2.3	Structure of the operator free space propagation with the angular spectrum of plane waves method. The initial disturbance $U(x, y; 0)$ is transformed into the angular spectrum $A(f_x, f_y; 0)$ with a Fourier transform implemented by a FFT algorithm. The angular spectrum is multiplied by the propagation transfer function $H(f_x, f_y)$ and the resultant angular spectrum is inverse transformed into the output disturbance $U(x, y; z)$. . .	42
2.4	example	43
2.5	example	45
2.6	Structure of the operator free space propagation with the angular spectrum of plane waves method in its band limmited version. The initial disturbance $U(x, y; 0)$ is transformed into the angular spectrum $A(f_x, f_y; 0)$ with a Fourier transform implemented by a FFT algorithm. The angular spectrum is multiplied by the propagation transfer function $H(f_x, f_y)$ whose bandwidth has been limited according to equation 2.63. The bandwidth of the transfer function depends by the sampling of the input field, by the wavelength of the light λ and of course by the propagation distance. The resultant angular spectrum is inverse transformed into the output disturbance $U(x, y; z)$. . .	46
2.7	The maximum spatial frequency is linked to the dimention of the sampling window of the output field w and the propagation distance z	47
2.8	exalmples	50
2.9	Comparison between the SNR as a function of the propagation distance for the three propagation method seen in section 2.4.1. The BL and the corrected BL methods improve the SNR, that instead drops with the increasing of the propagation distance when the normal AS method is used.	51
2.10	example	52
2.11	example	53
2.12	example	55
2.13	Phase profile of a computer generated lens. In Blue it is shown the unfolded quadratic phase term, in red the folded one, subject to aliasing.	56

2.14 Schematic of the 2f system simulated. f is the focal lenght, z the propagation distances, D is the aperture of the lens, w the field of view and N the sampling resolution.	59
2.15 Operator sequence for the 2f system.	60
2.16 From top to Bottom: Image and intensity cross section of a point source according to multi step method, angular spectrum method, band limited angular spectrum method and corrected band limited angular spectrum method.	63
2.17 From top left to bottom right: Power spectrum of the image of a point source obtained with the multi step Fresnel method, the Angular spectrum method, the band limited angular spectrum method and the corrected band limited angular spectrum method.	64
2.18 A random phase mask is generated propagating light coming form an array of sources, each one with a random phase value in the interval $[-\pi, \pi]$	69
2.19 Process of the creation of thephase mask. Top: array of point sources with a random phase value; centre: array of the areas of coherence afte the convolution with K ; bottom: randomized areas of coherence after the propagation of d_c	71
2.20 Final random phase mask generated by 10, 50, 100 and 200 sources.	72
2.21 Emission spectrum of the LED considered in our simulations and real image system.	73
2.22 example	75
2.23 Signal to noise ratio of the image of a USAF resolution target plotted as a function of the coherence index C	76
2.24 Images of the USAF resolution target with different values of ι . Increasing the number of point sources generating the phase mask creates improves the resolution and the contrast	77
2.25 Noise due to the speckles ini an image of a USAF resolution target after only 5 iterations.	78
2.26 Images of the USAF resolution target obtained adding an increasing number of snapshot. this is equivalent to increase the integration time of the sensor. As an effect of that the noise due to the speckles caused by the phase mask decreases.	79
2.27 Signal to noise ratio as a function of the number of iterations. The threshold has been calculated looking at the variance of the previous five data.	80
2.28	81

Chapter 1

Theory and methods of plenoptic imaging

1.1 Introduction

A camera is a device that captures light in a scene. [17]. Usually a conventional camera is composed by a detector and a lens. on the detector will be recorded the rays that passes through the aperture of the lens, forming a two dimensional irradiance map of the scene. Therefore a traditional traditional camera performs a special and restrictive sampling of the complete set of rays, and in general of the amount of information, contained in the the scene.[10]. It is interesting to define what is the total amount of information contained in the light captured by a camera and if there is an effective way to record and extract them. The space is filled with a dense array of light with various intensities [1]. from each point from the object imaged, a cone of rays departs and fill the whole space during the propagation. If a traditional camera is placed at a certain position from the object it fill sample only the cone of rays that are passing through its aperture. The information contained in this cone will than be recorded on a two dimensional plane

2 CHAPTER 1. THEORY AND METHODS OF PLENOPTIC IMAGING

losing information. To better quantify how much information is being lost by a conventional camera is worth to consider what kind of information is contained in a luminous environment. Following Adelson *et.al* [1], we will define a function, called plenoptic function, that contains all the information contained into the space. After that we will define a parametrization of the plenoptic function called Light Field, and we will explore a new class of optical instrument that are able to record and extract information from the light field. this class of instruments are called Computational cameras. They differ form a conventional camera because they are sample the light coming from the object in a radically different way, and are composed by a non conventional new optics that decode the light that hits the detector. This coded information is then decoded by a computational stage, in order to extract an image [10]. Schematics of the difference between a conventional and a computational camera can be found in figure 1.1

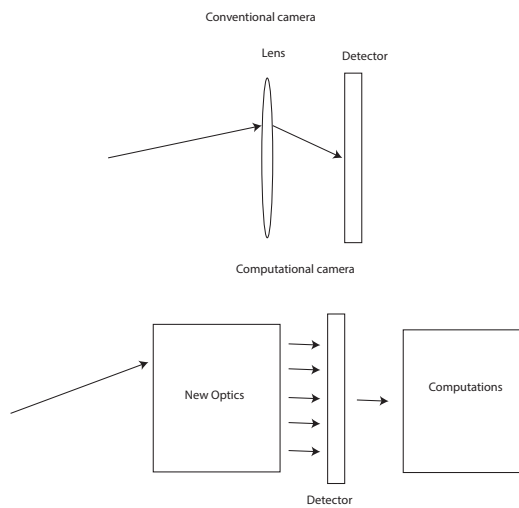


Figure 1.1: Differences between a traditional camera and a computational camera [10].

1.2 Plenoptic function and the light field

If we consider a black and white photographs taken by a conventional camera, it represents the intensity of light seen by a single viewpoint, at a single time, averaged over the wavelenghts of the visible spectrum [1]. For each point of the sensor, the intensituy can be represented bya function of the position $P(x, y)$. A color photograph adds information about the wavelength of the light, therefore we add a third variable, $P(x, y, \lambda)$.If we are taking a movie, the time dependence is added, $P(x, y, \lambda, t)$ and if the movie is captured using holographic techniques, i.e. saving phase and amplitude at of the optical field, we have information regarding the light intensity observable form any viewpoint $\vec{V} = (V_x, V_y, V_z)$. Therefore to describe the whole set of information that are potentially available contained into the light coming from the object we have a seven dimensional function. This function is called plenoptic function and its name comes from latin *plenum* that means full and *optica* that means optic.[2] [1]. The plenoptic function implicitly contain a description of every possible photography that can be taken of a particular scene from any possible points of view. To record the plenoptic function, one should move the camera along all the possible positions \vec{X} and take a snapshot, or having an array of cameras surrounding the object and taking snapshots simultaneously. The plenoptic function is an idealized concept and it is impossible to record it completely. However it is possible to record samples of it, or slices. For example a conventional black and white picture is a two dimensional slice along the coordinates x and y of the seven dimensional plenoptic function. It is taken from a single point of view, averaging the

4 CHAPTER 1. THEORY AND METHODS OF PLENOPTIC IMAGING

wavelength and integrating over the exposure time. A plenoptic camera is a camera that is able to record a section of the plenoptic function. In particular, a plenoptic camera records the part of the plenoptic function whose rays pass through the aperture of the camera. Therefore it records simultaneously all the possible viewpoints contained in the lens aperture. After having recorded the plenoptic function images are constructed by sectioning the plenoptic function. The process of extracting information from the plenoptic function is called rendering and it is where the computational stage operates. Before we proceed to describe a plenoptic camera it is useful to define another parametrization of the plenoptic function that is more useful to implement the computational algorithms in the next sections. We define light field as the radiance for unit of position and direction [9]. It can be described by a set of four coordinates. There are two possible representation of the light field: the two point representation and the point angle representation. With reference to figure 1.2 the two point parametrization states that if we consider a ray of light departing from point (x,y) , its direction of propagation in the three dimensional space is unequivocally defined by the couple of points where it crosses two parallel planes. Therefore the set of coordinates (x,y) and (u,v) defines only one ray of light. The point angle parametrization instead uses the coordinates of the point where the ray intercept a plane perpendicular to the optical axes, and the angles respect the optical axes along the directions x and y [4]. In both cases the intensity is a function of four coordinates. The 4D light field is therefore:

$$L(x, y, u, v) = L(x, y, \theta_x, \theta_y) \quad (1.1)$$

Where is shown the link between the two point parametrization and the point angle parametrization.

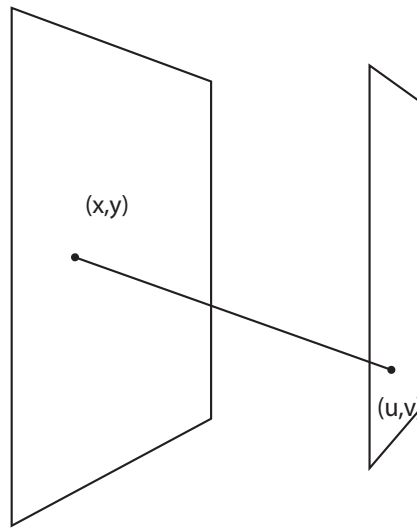


Figure 1.2: Two point representation of light field. Each ray of light is unequivocally defined by the coordinates of two points of interception.

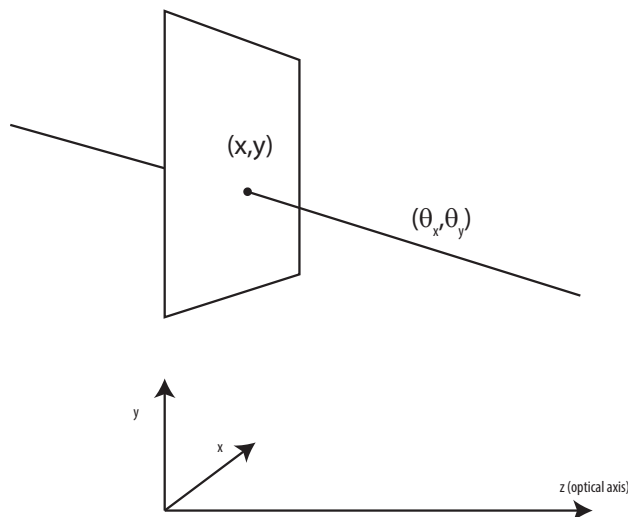


Figure 1.3: Point angle representation. A ray of light is unequivocally defined by the coordinates of a point that belongs to a plane perpendicular at the optical axis z and by the angles θ_x and θ_y that it forms with the optical axis along the directions x and y .

6 CHAPTER 1. THEORY AND METHODS OF PLENOPTIC IMAGING

A plenoptic camera records the light field, for each pixel on the sensor it is possible to determine the four coordinates: the spatial coordinates x, y and the directional coordinates θ_x, θ_y . Knowing the directional coordinates enables a set of computational features such as 3D reconstruction, synthetic refocus, full depth of field and aberration correction. Each of these features are possible after having decoded the light field with the computational stage shown in figure 1.1

1.3 Plenoptic camera

We now analyse an imaging system that is capable to record the light field. This system is called plenoptic camera. A plenoptic camera is a device designed for recording the 4D light field as described in equation 1.1. It is composed by a main lens with a defined aperture, a sensor and a micro lens array placed in front of the sensor [2]. The presence of the micro array allows to codify the directional information on the sensor. This coded image represents the raw data of the plenoptic camera. A model of the plenoptic camera can be seen in figure 1.4:

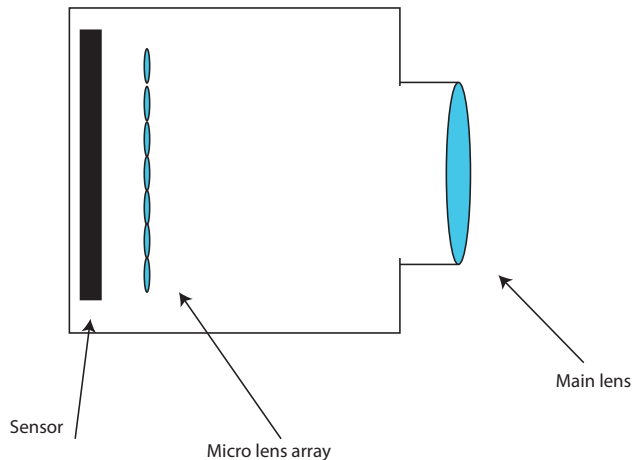


Figure 1.4: Plenoptic camera and its fundamental components. The presence of the micro array allows to record the light field .

The key component of the plenoptic camera is the micro lens array. From its design characteristics depend the optical performances of the camera. As explained in the introduction, the purpose of this project is to study the plenoptic camera under a wave optics approach in order to develop a plenoptic microscope for biomedical applications. The main issue with the micro lens array is its position respect the main lens and the sensor. According to where it is placed we can describe two types of cameras:

- if the main lens forms its image on the micro array and the micro lenses are focused on the sensor we have the first generation plenoptic camera, or plenoptic 1.0
- if the main lens forms its image on a plane that is different from micro array plane and the micro lenses image the main lens image plane on the sensor we have the focused plenoptic camera, or plenoptic 2.0

The two different kind of cameras can be seen in figure 1.5. In the next para-

8 CHAPTER 1. THEORY AND METHODS OF PLENOPTIC IMAGING

graph both configuration will be extensively analysed and it will be explained how they capture the light field with particular attention to the differences in the raw data they produce. It will also explained what are they performances in term of optical resolution, directional (or angular) resolution, axial resolution, and it will be discussed theyr suitability in term of biomedical applications. There will also be explained in detaill the computational algorithms to render images from the raw data.

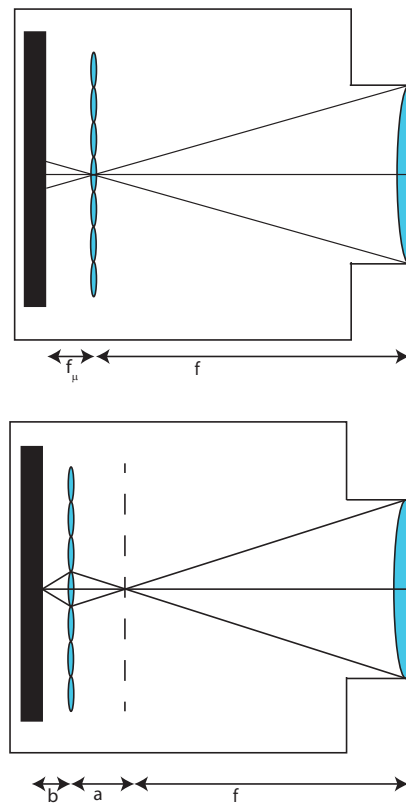


Figure 1.5: Top: Plenoptic camera 1.0. The main lens is focused at infinity, forms and image on the micro array and the micro array are is focused on the sensor. f is the focal length of the main lens and f_μ the focal length of the micro lens array. Bottom: Plenoptic camera 2.0. The main lens is focused at infinity and forms an image on the plane represented by the dashed line. The micro array acts as a relay between the main lens image and the sensor, since it satisfy the lens equation $1/a + 1/b = 1/f_\mu$.

1.4 Optical Phase Space

Before analysing the different configurations of plenoptic cameras, it is important to define an useful tools that allows to better represent the light field, in order to understand and manage it better. This is the optical phase space. In the representation of light field explained in section 1.2, each ray of the light field is defined by a set of four coordinates, two spatial coordinates x and y , and the directional coordinates θ_x and θ_y . Referring to figure we define momentum the quantity:

$$\vec{p} = \frac{\partial \vec{q}(s)}{\partial s} \quad (1.2)$$

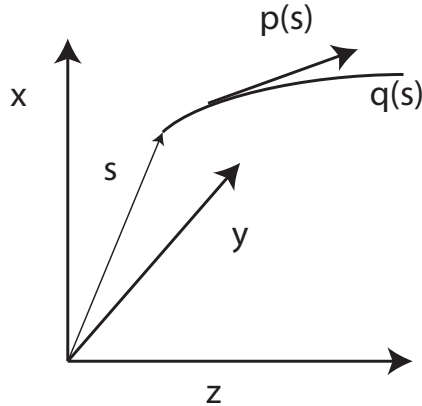


Figure 1.6: The optical momentum correspond to the direction of the ray of light.

where $\vec{q}(s)$ is a vector describing the trajectory of a ray of light in the three dimensional space and s is the position respect the origin of the axis x , y and z . Because of the Fermat principle, considering the trajectory of the ray $\vec{q}(s)$ as a straight line, its derivative is proportional to its angular coefficient. So we can approximate the momentum \vec{p} with the direction of the ray

(θ_x, θ_y) . It is defined as a four dimensional manifold of the positions (x, y) and momentum (p_x, p_y) of the rays in a certain volume [16] [8]. Each point in the phase space correspond to a unique ray. We will consider the phase space as a four dimensional manifold of the positions (x, y) and the directions (θ_x, θ_y) . For more details regarding the phase space refer to appendix A.

1.5 Plenoptic 1.0

The first version of the plenoptic camera has been proposed by Adelson and Wang in 1992 [2] and then improved by Ng *et.al* in 2006 [12] [11]. The purpose of Ng, was to design a camera that allows to use ray tracing techniques to compute synthetic photograph after the acquisition of the 4 dimensional light field. Following Adelson and wang idea, they never build a camera, bu only a prototype working with relay lense [12], Ng camera is made by an array of micro lenses placed in front of the sensor. Each micro lens forms an elemental sub image on the sensor. The directional information is collected using these sub images. The main lens focus the rays coming from one point in space on a single point in the image plane. If on the image plane an array of micro lenses is placed, all this rays will end up on a single micro lens. The micro lens will then split this bundle of rays on the sub image under it, allowing us to separate the rays according to their direction. This is explained in figure We consider the plenoptic camera as a simple 2 f system. The image plane is conjugate with the micro array plane, and the sensor plane is conjugate with the main lens image. Therefore under each micro lens, there will be a sub image that is an image of the main lens aperture. For simplicity only the system is composed by only three micro lenses and each sub image is

composed by only three pixels. The rays departing from a single point in the object plane, blue, red and green, are transferred by the main lens on a single micro lens. This micro lens then split up the rays. Each ray ends on a different pixel of the micro image.

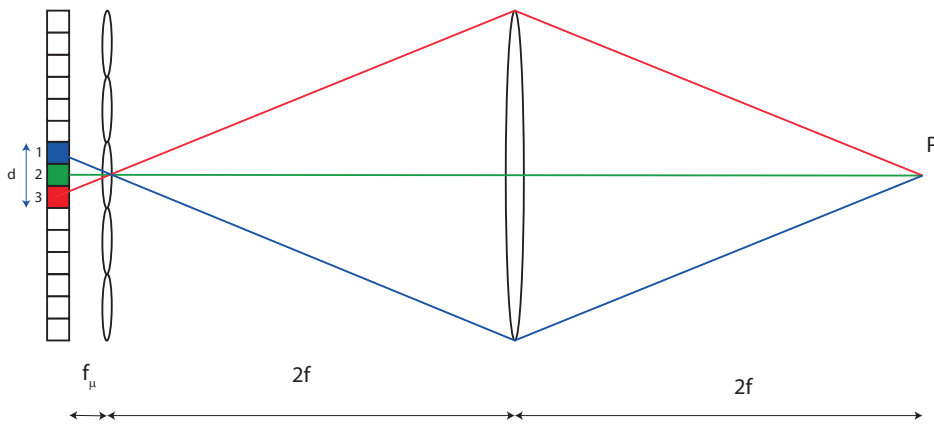


Figure 1.7: Ray diagram of a plenoptic 1.0 system. The main lens is in a $2f$ configuration respect the micro array. The sensor plane is conjugated with the main lens plane. The micro lens position maps the position (x,y) of the point P , while the sub image maps the directions of the rays coming from that point. The ray with direction θ_1 falls on the pixel 1 (blue), the ray with direction θ_2 falls on the pixel 2 (green) and the ray with direction θ_3 falls on the pixel 3 (red). The sub image d maps the direction of the ray.

In the example in figure 1.7 we only have three pixel per lens let. This means that the maximum number of direction that can be sampled is three. The number of directions that can be sampled by a plenoptic 1.0 camera are defined by the number of pixel under each micro lens. therefore we can state that the directional resolution is given by the sub image resolution. This implies an issue regarding spatial resolution. If we look again at figure 1.7 we can notice that the spatial position of the point P is recorded at the micro array plane. The sampling of the position is therefore linked to the

12CHAPTER 1. THEORY AND METHODS OF PLENOPTIC IMAGING

number of lens let in the micro array. This leads to a trade-off between directional and spatial resolution. Due to the finite dimension of the sensor, when using pixels to record the direction we loose pixel to record the position.

A further and more detailed explanation of this will be given in the next paragraph. Let's now look more in details how the light field is recorded. With reference to figure 1.8 we consider now three points at three different positions, but all belonging to the same plane in focus. We want now find a link between Levoy's definition of Light Field, the two point, or light slab, representation, and the output data of the plenoptic 1.0 camera. The sensor plane is conjugate to the main lens plane, while the micro array plane is conjugate to the object plane. Each sub image under each lens let will be an image of the main lens. The lens let plane is an image of the object plane and each lenslet correspond to a point in the object plane. To define the direction of a ray we need two point. One point is its origin, the second is where it crosses the main lens. But these two point are sampled by the lens let array and by the sub images on the sensor, as shown in figure 1.8. Therefore we can refer to the lens let position on the array with the coordinates spatial (x,y), and to the pixels of the sub images as the directional coordinates (u,v). With an array of 5 by 5 lens let and a sensor of 15 by 15 pixel, the 4D light field recorded will be a 5 by 5 by 3 by 3 function. Each point of this function is an intensity value identified by four coordinates, 2 spatial and 2 directional. the sampling of the spatial coordinates is 5 by 5, the sampling of the directional coordinates is 3 by 3.

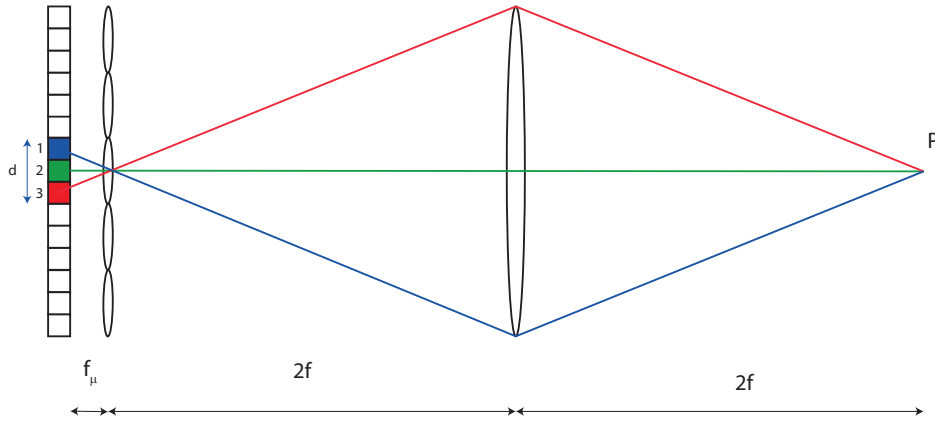


Figure 1.8: Ray diagram of a plenoptic 1.0 system. The main lens is in a $2f$ configuration respect the micro array. The sensor plane is conjugated with the main lens plane. The micro lens position maps the position (x,y) of the point P , while the sub image maps the directions of the rays coming from that point. The ray with direction θ_1 falls on the pixel 1 (blue), the ray with direction θ_2 falls on the pixel 2 (green) and the ray with direction θ_3 falls on the pixel 3 (red). The sub image d maps the direction of the ray.

This sampling is of course very low. The total number of direction to be sampled should be the ones of all the rays that enter the aperture of the main lens. The amount of light captured by a lens is defined by its f-number, defined as the ratio between the focal length and the aperture. We can also define the relative f number as the ratio between the distance between the lens and its image, and the aperture.

$$f_\# = \frac{z}{d} \quad (1.3)$$

where z is the distance from the main lens and the image plane and d its aperture. To be sure that all the directions sampled by the main lens are mapped into the light field, the f-number of the lens let should match the f-number of the main lens [12]. This condition known of f-number matching is very important in plenoptic imaging. If the f-number of the lens let is smaller

than the one of the main lens then there is an under sampling of the rays intercepted by the main aperture, as well as a waste of pixel that remains dark. If the f-number of the lens let is bigger on the other hand there is cross-talk between the sub images, having loss of data. The f-number matching can be seen in figure 1.9

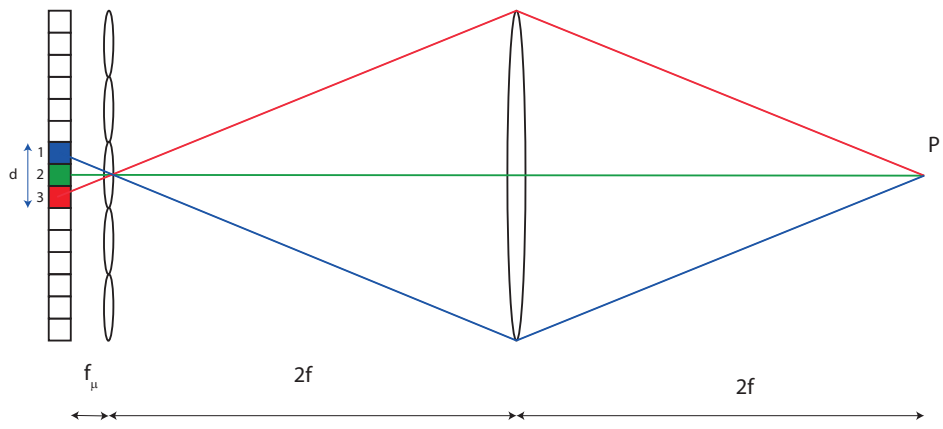


Figure 1.9: F-number matching between the main lens and the micro lens in the array.

1.5.1 Phase space in plenoptic 1.0

it is very useful to analyse the sampling of the light field under a phase space point of view. In figure a point source is sampled by the lens let array. We consider the mono dimensional case for simplicity. The single ray departing from the point P on the focal plane of the main lens is refracted by the optical system and hits a pixel of a specific sub image on the sensor. The sub image position on the array gives the coordinate x . The pixel of the sub image gives the direction θ_x . In the phase space a single ray is represented by a single point.

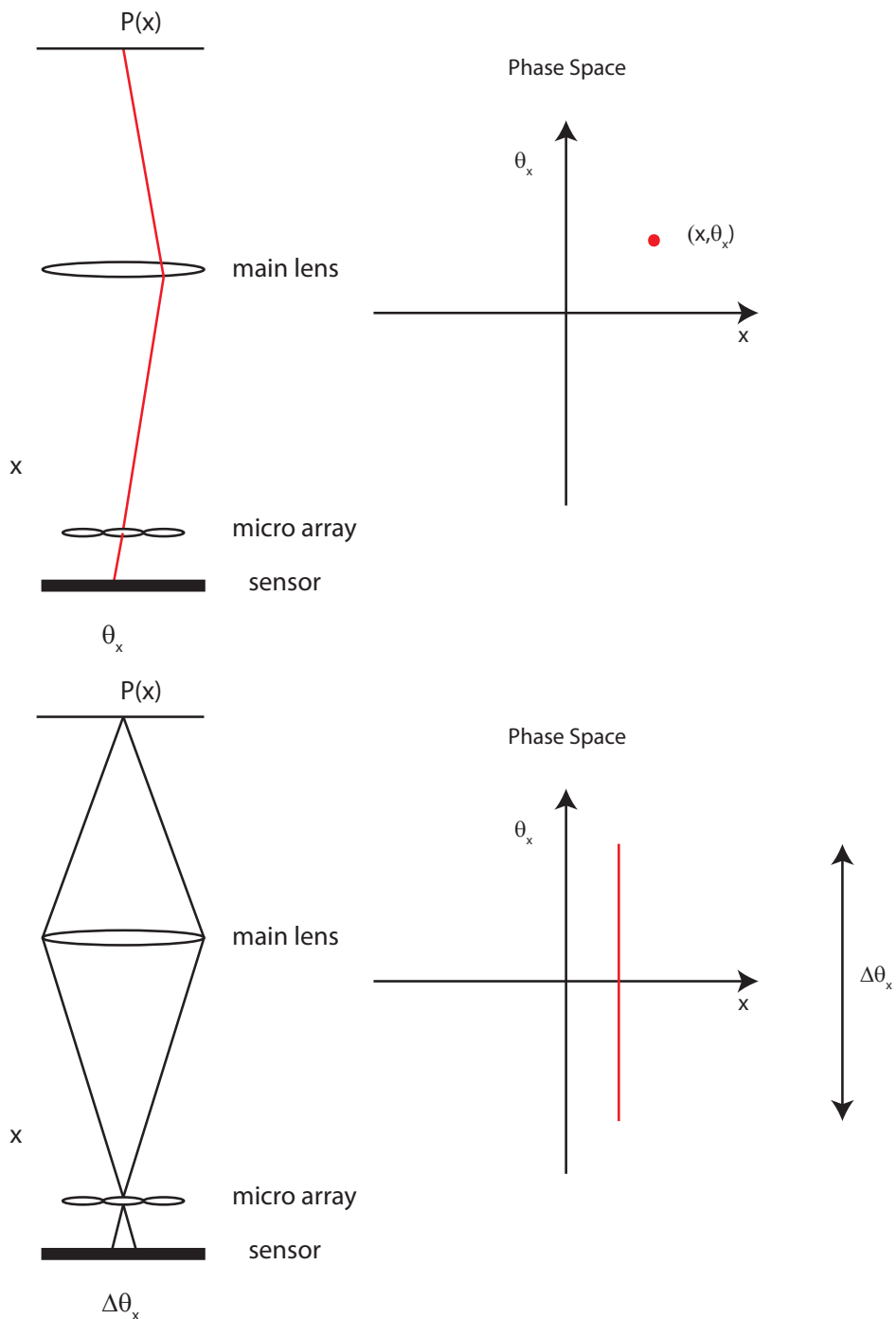


Figure 1.10: Sampling of the light field and phase space representations of the rays.

16CHAPTER 1. THEORY AND METHODS OF PLENOPTIC IMAGING

If we consider the full range of possible directions of the rays captured by the main lens, they will all be focused on a single lens let and then split on the sub image. Each pixel of the sub image corresponds to a different direction. In the phase space this is equivalent to a vertical line. One position x and $\Delta\theta_x$ possible directions. The range $\Delta\theta_x$ is defined by the numerical aperture of the main lens, m matched with the one of the lens let.

1.5.2 Light Field Parametrization

Before discussing the rendering procedures for plenoptic 1.0 light field data, we introduce three different parametrization of the light field from the raw image. A plenoptic 1.0 raw image looks like an array of sub images, each sub image contains samples of direction. An example of a plenoptic raw image can be seen in figure 1.11, while in figure 1.12 it is shown in detail how a sub image appears. The raw image has been generated simulating light propagating into a plenoptic camera composed by a 60 mm lens, with an aperture of 7 mm, and a sensor with a resolution of 1500 by 1500 pixel. the micro array is composed by 75 by 75 lens let with a focal length of 5 mm.

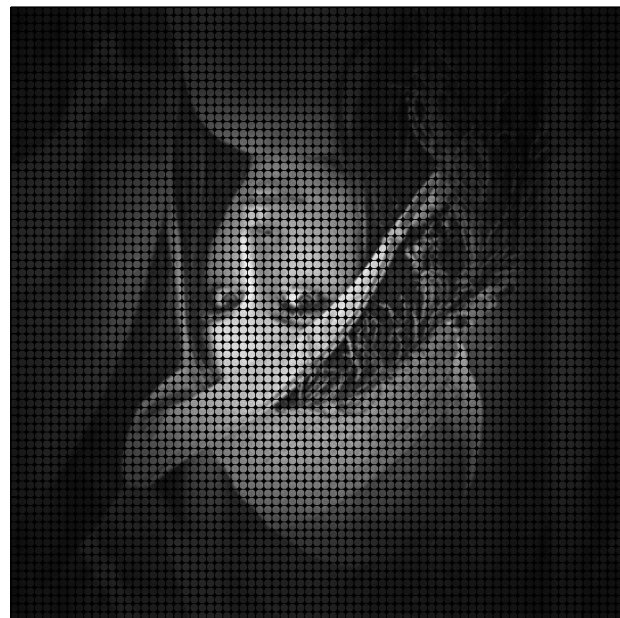


Figure 1.11: Example of a raw plenoptic 1.0 image.

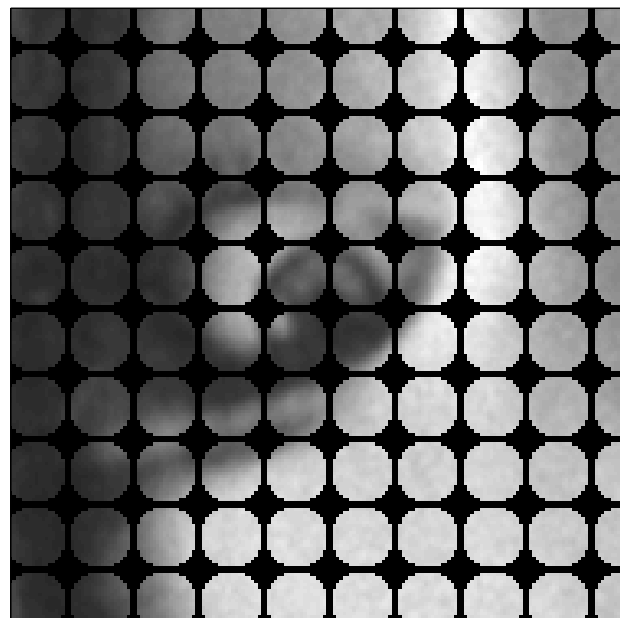


Figure 1.12: Zoom on the raw image. Each lenslet is formed by 20 by 20 pixels. each pixel represent a direction of the rays hitting the lens let that produced the sub image.

18CHAPTER 1. THEORY AND METHODS OF PLENOPTIC IMAGING

This first raw image is already the first parametrization of the light field and it is called camera view. Pixels are arranged according to the positional coordinates, and each sub image contains the directional coordinates. A second parametrization, known as array view, is obtained rearranging the pixel according the directional coordinates. The result is an array of N by N sub images, where N is the number of samples of the directional coordinates, where each sub image represents the point of view linked with a direction (θ_x, θ_y). The array view can be seen in figure while the method to pass from the camera view to the array view is illustrated in figure

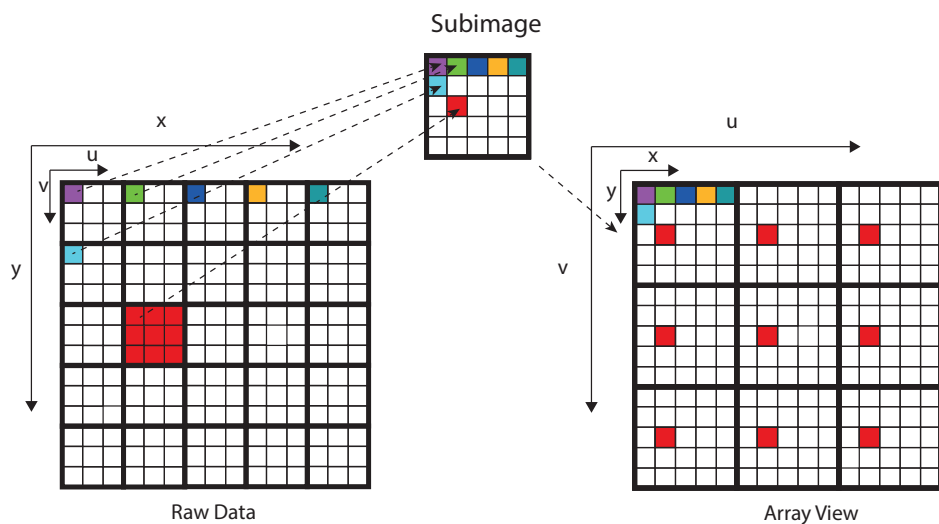


Figure 1.13: The array view is an array of the different point of view obtained rearranging the pixel according to the directional coordinates.

An example of the array view parametrization of the raw image in figure 1.11 is shown in figure 1.14.

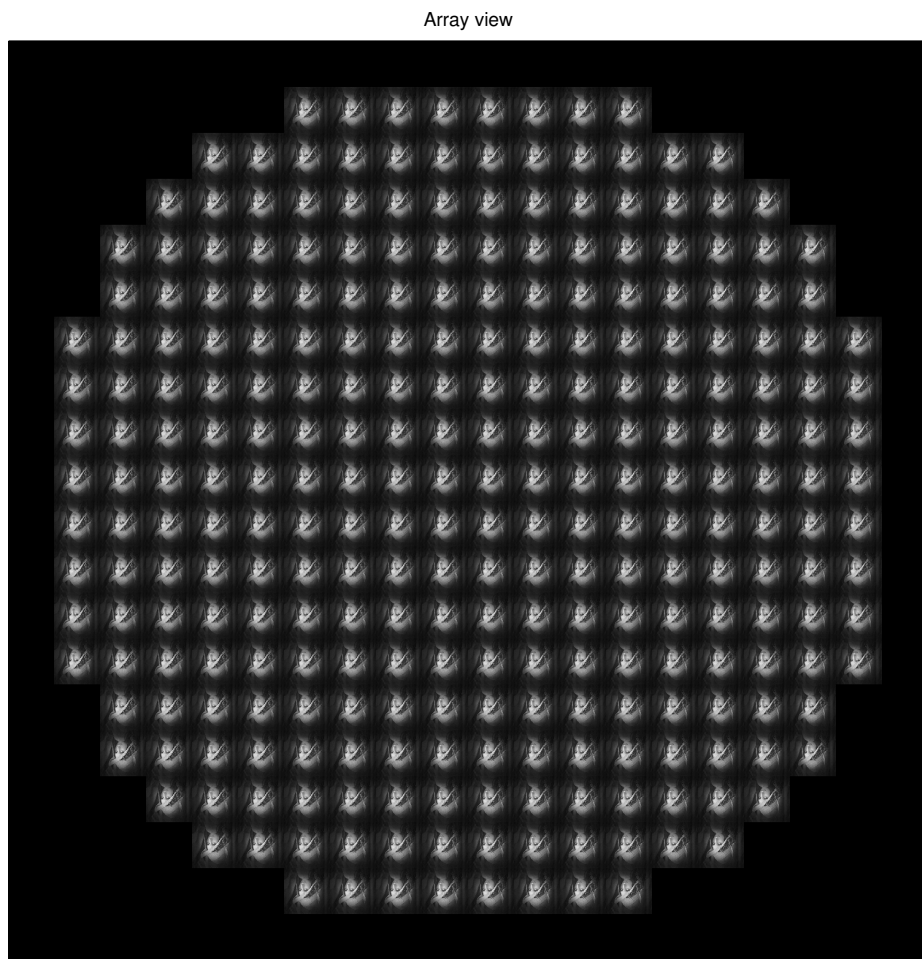


Figure 1.14: The array view is an array of the different point of view obtained rearranging the pixel according to the directional coordinates.



Figure 1.15: Zoom of the central part of the array view showing in detail the different point of views .

The third and last parametrization of the light field, is the 4 D radiance, that can be represented as the phase space. This third parametrization is less intuitive but is very useful from a computational point of view since it is a four dimensional array, and every ray can be addressed by a set of four coordinates, or indices, as will be explained in detail in chapter 3.

1.6 Plenoptic 1.0 rendering

The act of de-codifying the information present on the sensor of the plenoptic camera in order to get an image is called rendering. The sensor raw image looks like an array of sub-images. Each sub image contains stored the directional information of the rays coming from a point in the scene mapped by the the correspondent micro lens. A conventional 2D image is captured integrating for any position all the rays converging on that point as shown in figure

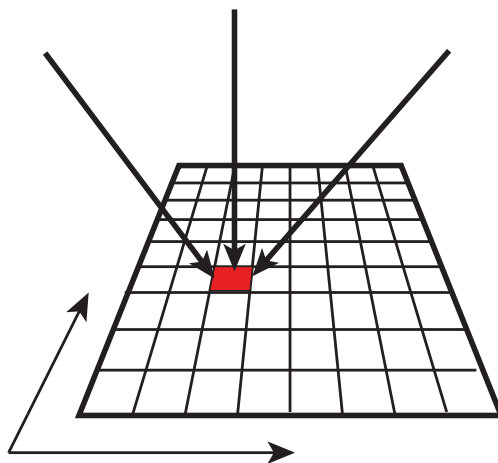


Figure 1.16: Sampling of the light field and phase space representations of the rays.[11]

Therefore, if $L(x, y, u, v)$ is the sampled 4D light field, represented with the two point convention, the radiance $E(x, y)$ on a pixel (x, y) of the conventional image will be given integrating all the rays coming from all the sampled directions (u, v) . Following the work of Ng *et.al* [11] we have:

$$I(x, y) = \frac{1}{z^2} \iint L(x, y, u, v) A(u, v) \cos^4 \Theta du dv \quad (1.4)$$

Where z is the distance between the main lens and the sensor, Θ is the angle formed by the rays and the sensor normal and $\cos^4 \Theta$ is the vignetting factor that take into account the reduced effects of the rays striking the sensor from oblique directions. $A(u, v)$ is an aperture function that limits the direction upon we are integrating to the ones included in the aperture of the main lens. Under a condition of paraxial approximation, we can drop the $\cos^4 \Theta$ term as well as the $1/z^2$ term. The equation 1.4 then becomes:

$$I(x, y) = \iint L(x, y, u, v) A(u, v) dudv \quad (1.5)$$

From a computational point of view, since we deal with discreet samples of the light field, the double integral is implemented as a double sum along the directional coordinates. The total intensity of each pixel of the rendered image is then the sum of the intensities of the pixels that form the correspondent sub image. For a light field with N by N directional samples, the intensity of the rendered image $I(x, y)$ is given by:

$$I(x, y) = \frac{1}{N^2} \sum_{i=0}^N \sum_{j=0}^N L(x, y, i, j) \quad (1.6)$$

This can be seen very clearly in the phase space where each pixel of the final image is made by the sum of all the directional samples [5], as shown in picture 1.17. The total range of directions defined by the numerical aperture of the main lens is sampled by N by N pixels.

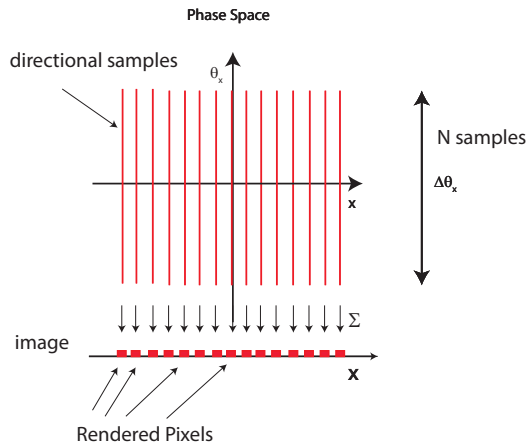


Figure 1.17: Rendering seen from the (x, θ_x) slice of the phase space. [5]

rendering an image from a light field captured by a plenoptic 1.0 camera causes a loss of resolution if compared with the image collected by a conventional camera using the full sensor. If we consider a plenoptic camera composed by a sensor with a resolution of 1000 by 1000 pixels and a micro lens array of 100 by 100 lens let, each sub image will contain 10 by 10 directional samples. All this samples will contribute in computing the intensity of a single pixel, therefore we will have only one pixel per lens let in the final image. The rendered image will have a resolution of 100 by 100 pixel. This is the main limitation to plenoptic 1.0 cameras, the better the directional information are sampled, the more spatial resolution is lost. [5] [11]. An example of a rendered image from a computer generated light field is shown in figure 1.18



Figure 1.18: rendered image form the raw data in figure 1.11. Resolution is only 75 by 75 pixel. [5]

1.6.1 Changing Aperture and point of view

During the rendering stage it is possible to do some post processing transformation rearranging the data contained in the light field. We will present two of these possible features: change of aperture and change of point of view. If we look at the raw plenoptic image, each sub image is formed by a number of samples of the directions of the rays. If in equation 1.5 we reduce the range of integration along the directional coordinates, this is equivalent in reducing the aperture of the main lens, since less rays will be considered to form the intensity of each pixel. The result is a rendered image that looks like it has been captured with a narrower aperture, therefore with less light. From a

computational point if we want to reduce the aperture of a k pixels we have:

$$I(x, y) = \frac{1}{N'^2} \sum_{i=k/2}^{N-\frac{k}{2}} \sum_{j=k/2}^{N-\frac{k}{2}} L(x, y, i, j) \quad (1.7)$$

where $N' = N - k$. This operation in the phase space is shown in figure:

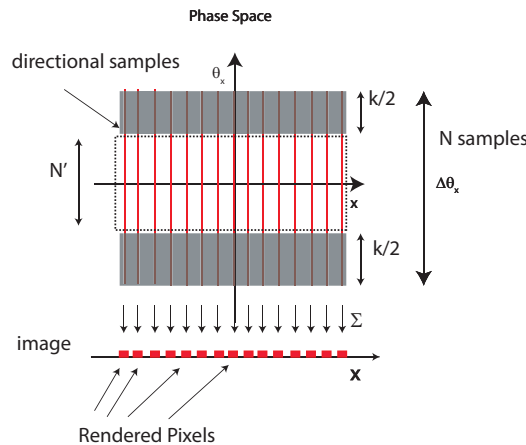


Figure 1.19: Rendering seen from the (x, θ_x) slice of the phase space. In grey are shown the directional pixels not considered for the integration.

Two examples of imaged rendered changing the aperture in post processing can be seen in figure 1.20.

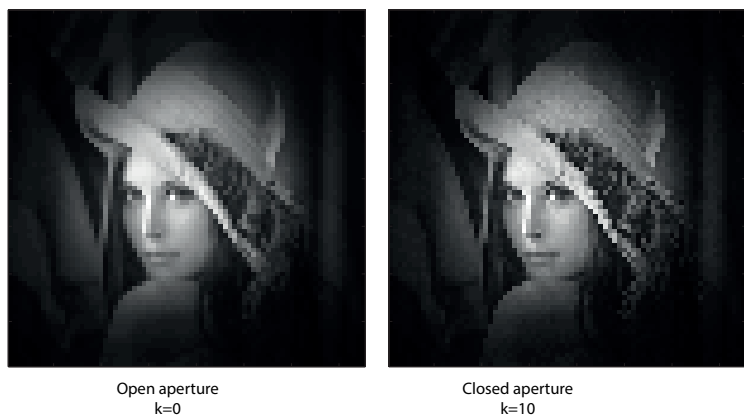


Figure 1.20: Rendering seen from the (x, θ_x) slice of the phase space. In grey are shown the directional pixels not considered for the integration.

Selecting the directional components to integrate is possible to change to point of view of the rendered image, in the limit of the directions contained in the f-number of the main lens. Viewpoint can be chosen both in x and y direction. It is possible to choose only one specific viewpoint (θ_x, θ_y) , that rendering the image using only one single pixel per sub image, as shown in figure, or it is possible to select a point on view in θ_x or θ_y and integrate over all the other direction. The rendering equation then becomes:

$$\begin{aligned} I(x, y) &= \frac{1}{N} \sum_{i=0}^N L(x, y, i, \theta_y) \\ I(x, y) &= \frac{1}{N} \sum_{j=0}^N L(x, y, \theta_x, j) \end{aligned} \tag{1.8}$$

1.7 Synthetic refocus

1.8 Depth estimation

Chapter 2

Fresnel Simulation Toolbox

2.1 Introduction

Considered the complexity of the system studied, the development of a tool to study its optical properties in order to design a working prototype has been necessary. This tool had to follow the following requirements:

- It had to preserve the phase of the optical field coming from the object for all the propagation path inside the optical system in order to preserve directional information
- It had to permit an analysis of the system at its diffraction limit
- It had to be simple and versatile, in order to easily change the characteristic of the optical system, trying various configurations

To address these features, was decided to develop a simulation toolbox on MATLAB, to propagate light under a wave optics approach. Most of the works done simulating plenoptic system are based on ray tracing techniques. The advantages of using ray tracing are that using geometrical optics approach linear operators can be defined in order to perform transformations

on the bundle of rays. These operators are the free space propagation and the lens operator. In developing the model of Light propagating into the optical system we will assume that the all the media composing the system are linear, isotropic, homogeneous and non dispersive. We will explain this properties in the following section

2.2 Scalar Theory of diffraction

For the theory of scalar diffraction, that is the basis of the simulation platform developed, we will follow Goodman derivation [6]. The start point for to study an optical fields propagating into an optical system is given by Maxwell Equations in absence of sources of the electrical field of of magnetic dipoles:

$$\begin{aligned}\nabla \times \vec{E} &= -\mu \frac{\partial \vec{H}}{\partial t} \\ \nabla \times \vec{H} &= \epsilon \frac{\partial \vec{E}}{\partial t} \\ \nabla \cdot \epsilon \vec{E} &= 0 \\ \nabla \cdot \mu \vec{B} &= 0\end{aligned}\tag{2.1}$$

\vec{E} is the electric field, \vec{H} is the magnetic field, μ and ϵ are respectively the magnetic permeability and electrical permittivity of the medium in which the optical wave is propagating. Both \vec{E} and \vec{H} are a function of the position x, y and z , as well as the time t . The operator ∇ is defined as:

$$\nabla = \frac{\partial}{\partial x} \hat{i} + \frac{\partial}{\partial y} \hat{j} + \frac{\partial}{\partial z} \hat{k}\tag{2.2}$$

where \hat{i}, \hat{j} and \hat{k} are the unit vectors along the directions x, y and z . We assume the wave propagating in a dielectric medium that is linear, isotropic and homogeneous. A medium is linear if its response to a several disturbances acting simultaneously can be decomposed into the sum of the responses to the single disturbance individually. It is isotropic if its properties do not depends on the directions of polarization of the wave and is homogeneous if its permittivity is constant along all direction of propagation. The medium is considered also to be non dispersive, that is the permittivity *epsilon* is not dependent by the wavelength. We apply now the operator $\nabla \times$ ont he left and on the right side of the first equation of 2.1. Using the vector identity

$$\nabla \times (\nabla \times \vec{E}) = \nabla(\nabla \cdot \vec{E}) - \nabla^2 \vec{E} \quad (2.3)$$

we have:

$$\nabla(\nabla \cdot \vec{E}) - \nabla^2 \vec{E} = \nabla \times (-\mu \frac{\partial \vec{H}}{\partial t}) \quad (2.4)$$

From the third equation in 2.1:

$$\nabla \cdot \epsilon \vec{E} = 0 \quad (2.5)$$

then the equation 2.4 becomes:

$$-\nabla^2 \vec{E} = \nabla \times (-\mu \frac{\partial \vec{H}}{\partial t}) \quad (2.6)$$

since both the operators $\nabla \times$ and derivative are linear we have swapped them on the righthand side of equation 2.4. Then substituting equation the second Maxwell equation 2.1 into the 2.6 we have

$$-\nabla^2 \vec{E} = -\mu \epsilon \frac{\partial^2}{\partial t^2} \vec{E} \quad (2.7)$$

The operator ∇^2 is the Laplacian operator and is defined as:

$$\nabla^2 = \frac{\partial^2}{\partial x^2} \hat{i} + \frac{\partial^2}{\partial y^2} \hat{j} + \frac{\partial^2}{\partial z^2} \hat{k} \quad (2.8)$$

We define the refractive index of the medium in which the wave is propagating as:

$$n = \sqrt{\frac{\epsilon\mu}{\epsilon_0\mu_0}} \quad (2.9)$$

where ϵ_0 is the permittivity of the vacuum and μ_0 the magnetic permeability in vacuum. Also, defining the speed of light in the vacuum as:

$$c = \sqrt{\frac{1}{\epsilon_0\mu_0}} \quad (2.10)$$

Then the wave equation for the electric field is:

$$\nabla^2 \vec{E} - \frac{n^2}{c^2} \frac{\partial^2 \vec{E}}{\partial t^2} = 0 \quad (2.11)$$

Same considerations can be done for the magnetic field, leading to an identical equation:

$$\nabla^2 \vec{H} - \frac{n^2}{c^2} \frac{\partial^2 \vec{H}}{\partial t^2} = 0 \quad (2.12)$$

Since the wave equation is obeyed both by the electric field and the magnetic field, it is possible to define a scalar wave equation, obeyed by the single components of those vectors. We represent the scalar field components as a function $u(x, y, z, t)$ dependent both from the position in space (x, y, z) and time t . u is the called field disturbance. The scalar wave equation is:

$$\nabla^2 u - \frac{n^2}{c^2} \frac{\partial^2 u}{\partial t^2} = 0 \quad (2.13)$$

With this scalar approximation it is possible to treat the propagation of an optical field as a scalar. this is only valid under the assumption of a linear,

isotropic, homogeneous and non dispersive medium, since all the component in all the directions of the electric and magnetic fields must behave identically.

2.2.1 Helmotz equation

We consider now the case of monochromatic wave. The scalar field u is then:

$$u(\vec{X}, t) = A(\vec{X}) \cos[2\pi\nu t - \phi(\vec{X})] \quad (2.14)$$

$A(\vec{X})$ is the amplitude of the disturbance and $\phi(\vec{X})$ is its phase at point in the space with coordinates $\vec{X} = (x, y, z)$. It can be written separating the time and space dependence:

$$u(\vec{X}, t) = \operatorname{Re} U(\vec{X}) e^{-j2\pi\nu t} \quad (2.15)$$

where U is a complex function of position and includes the phase term.

$$U(\vec{X}) = A(\vec{X}) e^{j\phi(\vec{X})} \quad (2.16)$$

This scalar field should satisfy the scalar wave equation 2.13. We have:

$$\nabla^2 [U(\vec{X}) e^{-j2\pi\nu t}] - \frac{n^2}{c^2} \frac{\partial^2}{\partial t^2} [U(\vec{X}) e^{-j2\pi\nu t}] = 0 \quad (2.17)$$

Doing the derivatives and simplifying the exponential terms we get:

$$\nabla^2 [U(\vec{X})] + \left(\frac{2\pi\nu n}{c} \right)^2 [U(\vec{X})] = 0 \quad (2.18)$$

Since the wave number is:

$$k = \frac{2\pi\nu n}{c} \quad (2.19)$$

we can write the expression 2.18 in a more compact form:

$$(\nabla^2 + k^2) U = 0 \quad (2.20)$$

The 2.20 is the z equation. It describe the behaviour of a complex disturbance propagating in a homogeneous medium. All the approximations of the optical field must obey this equation.

2.2.2 Solutions of Helmholtz Equations

We consider now the problem of diffraction of light by an aperture. Calculation of a analytical expression of the complex disturbance U that satisfies the Helmholtz equation can be done using the green's theorem under particular boundaries condition as explained by Goodman. There are two possible solutions: Fresnel-Kirchhoff and Rayleigh-Sommerfeld. Considering a wave U_0 propagating through a diffracting screen at a point in space with coordinates $z = 0$ with an aperture D we can define the following boundaries conditions:

- Fresnel-Kirchhoff (FK) conditions

$$U(x, y, 0) = U_0(x, y, 0) \text{ for } (x, y) \in D$$

$$U(x, y, 0) = 0 \text{ for } (x, y) \notin D$$

$$\frac{\partial U}{\partial z} = \frac{\partial U_0}{\partial z} \text{ for } (x, y) \in D$$

$$\frac{\partial U}{\partial z} = 0 \text{ for } (x, y) \notin D$$

- Rayleigh-Sommerfeld (RS) conditions:

$$U(x, y, 0) = U_0(x, y, 0) \text{ for } (x, y) \in D$$

$$U(x, y, 0) = 0 \text{ for } (x, y) \notin D$$

] The FK conditions lead to a simple result but they are not physically correct since they imply that the field after the screen to decay to zero outside of the aperture in the immediate proximity of the screen as well as its normal derivative. Results are accurate only for a distance from the aperture much bigger than the wavelength. The RS condition on the other hand made is less strict since regards only the value of the disturbance after the screen. Therefore we will only consider the RS solution of the Helmholtz equation. The disturbance generated by the diffraction ta a distance z by the aperture that is:

$$U(x, y, z) = \frac{1}{j\lambda} \int \int_{\sigma} U(\xi, \eta, 0) \frac{e^{jkr}}{r} \cos(\theta) d\xi d\eta \quad (2.21)$$

where, with reference to figure 2.1, θ is the angle between the z axis and the direction of propagation, $r = \sqrt{z^2 + (x - \xi)^2 + (y - \eta)^2}$ is the distance between the point $P_1 = (x, y, z)$ and $P_0 = (\xi, \eta, 0)$ and σ is the area of aperture. Since $\cos(\theta) = \frac{z}{r}$ we have: that is:

$$U(x, y, z) = \frac{z}{j\lambda} \int \int_{\sigma} U(\xi, \eta, 0) \frac{e^{jkr}}{r^2} d\xi d\eta \quad (2.22)$$

Figure 2.1: example

2.2.3 The Fresnel Approximation

It is possible to approximate the distance of propagation r between P_0 and P_1 with its Taylor expansion at the second order:

$$r = \sqrt{1 + \left(\frac{x - \xi}{z}\right)^2 + \left(\frac{y - \eta}{z}\right)^2} \approx z \left[1 + \frac{(1)}{2} \left(\frac{x - \xi}{z}\right)^2 + \frac{1}{2} \left(\frac{y - \eta}{z}\right)^2 \right] \quad (2.23)$$

Therefore for large propagation distances, that is $z \gg x, y$ the diffraction integral becomes:

$$U(x, y) = \frac{e^{jkz}}{j\lambda z} \int \int_{-\infty}^{\infty} U(\xi, \eta) e^{\frac{jk}{2z}[(x-\xi)^2 + (y-\eta)^2]} d\xi d\eta \quad (2.24)$$

Factorizing the exponential term in the integral we obtain that the disturbance $U(x, y)$ after in a plane (x, y) at a distance z from the input disturbance at the plane (ξ, η) is:

$$U(x, y) = \frac{e^{jkz}}{j\lambda z} e^{j\frac{k}{2z}(x^2+y^2)} \int \int_{-\infty}^{\infty} U(\xi, \eta) e^{\frac{jk}{2z}(\xi^2+\eta^2)} e^{\frac{-jk}{2z}(x\xi+y\eta)} d\xi d\eta \quad (2.25)$$

That can be seen as the Fourier transform of the disturbance before the aperture $U(\xi, \eta)$ multiplied by a quadratic phase factor $e^{\frac{jk}{2z}(\xi^2+\eta^2)}$.

2.3 Operator Free space propagation: Fresnel Approximation approach

The first version of the operator free space propagation has been developed using the Fresnel Integral has written in equation 2.25. The input disturbance $U(\xi, \eta)$ is considered to be illuminated by monochromatic light with wavelength λ . As stated in section 2.3 the Fresnel integral can be seen as the two dimensional Fourier transform of the input field $U(\xi, \eta)$ multiplied by a quadratic phase factor. This is going to be very useful from a computational point of view since it can be implemented with a fast fourier transform algorithm (FFT). We define the function $U'(\xi, \eta)$:

$$U'(\xi, \eta) = U(\xi, \eta) e^{\frac{jk}{2z}(\xi^2+\eta^2)} \quad (2.26)$$

Therefore the optical field at the plane z is the product of the Fourier transform of $U'(\xi, \eta)$ for the phase term $e^{\frac{ik}{2z}(x^2+y^2)}$:

$$U(x, y) = \frac{e^{ikz}}{i\lambda z} e^{\frac{ik}{2z}(x^2+y^2)} \mathcal{F}[U'(\xi, \eta)] \quad (2.27)$$

where the spatial frequencies of the Fourier Transform can be correlated with the spatial coordinates x and y by the relation:

$$\begin{cases} \nu_x = \frac{x}{\lambda z} \\ \nu_y = \frac{y}{\lambda z} \end{cases} \quad (2.28)$$

This is computationally fast since require only one fourier transform, and is analytically correct. Particular attention should be given to the sampling of the the optical field U and U' . Becaouse of the nature of the nature of the presence of the Fourier transform the the coordinates of the input and output fields are not sampled in the same way, but are scaled of a factor that is proportional to the distance of propagation, as shown in equation 2.28. Therefore the output plane should be sampled with a frequency that is different then the input one [13]. In addition to that, the multiplicative phase factor:

$$e^{\frac{ik}{2z}(\xi^2+\eta^2)} \quad (2.29)$$

presents the propagation distance at the denominator of the exponential, leading to rapid oscillation of the phase of the optical field for small variations of z . In order to avoid aliasing is therefore necessary a large sampling frequency of the input field, that is a large resolution of the object field. It is known that the computational effort of the FFT algorithm increases with the resolution with a relation that is $O(n \log n)$, where n is the number of samples of the input field. To overcome these issues a modified method has been developed.

2.3.1 Multi-Step Fresnel propagation operator

We uses a multi step approach as the one explained by Sypek *et.al* [13][14] and as its shown in figure ?? . While Sypek *et.al* develop a multistep prop-

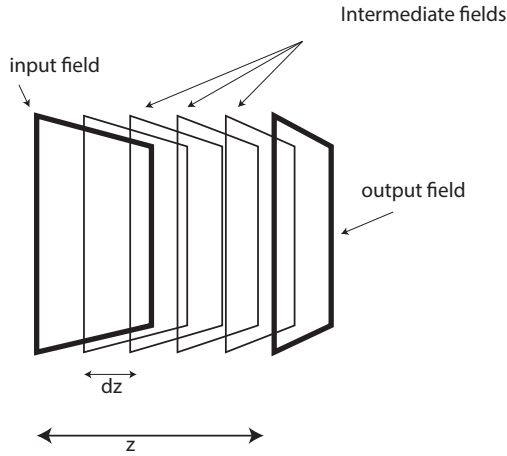


Figure 2.2: To remove the scaling factor between the input and output fields, we developed a multi step Fresnel approach. The field is propagated by unit of dz , the minimum distance to keep the sampling the same.

agatiuon model to minimize the oscillations of the Fourier spectrum of the Fresnel integral in order no to enanche the sampling with a zero padding, our approach is focused in removing the scaling factor between the input field and the output field that arise froen the Foourier transform as shown in eequation 2.28. When we go into the Fourier domain, if the sampling of the input field is $N \times N$, dx is the pixel size in meters of the input field and $d\nu$ is the spatial frequency resolution so that the pixel size in the image plane is:

$$d\xi = d\nu\lambda z \quad (2.30)$$

where z is the propagation distance. The condition to keep the same resolution both in the input field and the output field is:

$$d\xi = d\nu\lambda z = dx \quad (2.31)$$

Since the resolution in spatial frequency is given by

$$d\nu = \frac{1}{Ndx} \quad (2.32)$$

Substituting the 2.32 into the 2.28 and considering that $d\xi = dx$ we have that the condition to keep the resolution is:

$$\frac{1}{Ndx} = \frac{dx}{\lambda z} \quad (2.33)$$

Then resolving for z we have the minimum propagation distance to keep the same sampling both in the input and output fields: $d\xi = dx$ we have that the condition to keep the resolution is:

$$dz = \frac{W^2}{N\lambda} \quad (2.34)$$

and we have:

$$z = \sum_{i=1}^N dz_i \quad (2.35)$$

Where $W = Ndx$ is the dimension in meters of the input field. The equation 2.34 gives the length of the single step in which the propagation distance z should be divided in order to keep the same resolution. Although the results obtained with this multi-step approach are correct and noise is reduced, there are some issues. The first practical issue is that the propagation distance should be a multiple of dz , and this is an enormous limitation to our research, since in plenoptic imaging systems it is important to know

the propagation distances with extreme precision. The second issue regards the computational time. With the multi step approach the number of FFT performed increases with the number of steps, leading to an increase in computational time. For these reasons we abandoned the multi step approach to switch to the angular spectrum method as will be discussed in section 2.4.

2.4 Operator Free space propagation: Angular spectrum of plane waves approach

The operator free space propagation can be derived treating diffraction as a linear system with a transfer function that has a bandwidth that is proportional to the distance of propagation. The input disturbance can be analysed in the Fourier domain considering all Fourier components as plane waves travelling in different directions. This approach to propagation problem is called Angular Spectrum of Plane waves approach. It is possible then define the operator propagation as a linear system with a characteristic transfer function.[6]

2.4.1 Angular spectrum of plane waves

We consider a monochromatic wave incident a plane (x,y) while travelling along the z direction. At the plane $z=0$ the disturbance $U(x, y; 0)$ has a Fourier transform given by:

$$A(f_x, f_y; 0) = \int \int_{-\infty}^{\infty} U(x, y; 0) e^{-j2\pi(f_x x + f_y y)} dx dy \quad (2.36)$$

and $U(x, y; 0)$ is equal to the inverse Fourier transform of its spectrum:

$$U(x, y; 0) = \int \int_{-\infty}^{\infty} A(f_x, f_y; 0) e^{j2\pi(f_x x + f_y y)} df_x df_y \quad (2.37)$$

2.4. OPERATOR FREE SPACE PROPAGATION: ANGULAR SPECTRUM OF PLANE WAVES A

The physical meaning of the equation 2.37 is that the disturbance $U(x, y; 0)$ can be decomposed in the sum of elemental plane waves propagating in directions given by the wave vector \vec{k} whose magnitude is $2\pi/\lambda$ and direction is given by its direction cosines (α, β, γ) . Dropping the temporal dependence the plane wave is then:

$$p(x, y, z) = e^{-j\vec{k} \cdot \vec{r}} \quad (2.38)$$

where

$$\vec{r} = x\hat{i} + y\hat{j} + z\hat{k} \quad (2.39)$$

and

$$\vec{k} = \frac{2\pi}{\lambda}(\alpha\hat{i} + \beta\hat{j} + \gamma\hat{k}) \quad (2.40)$$

The exponential becomes:

$$p(x, y, z) = e^{-j\frac{2\pi}{\lambda}(\alpha x + \beta y)} e^{-j\frac{2\pi}{\lambda}(\gamma z)} \quad (2.41)$$

The relation between the direction cosines is:

$$\gamma = \sqrt{1 - \alpha^2 + \beta^2} \quad (2.42)$$

Therefore the complex exponential function in equation 2.36 can be seen as a plane wave with direction cosines

$$\alpha = \lambda f_x, \quad \beta = \lambda f_y, \quad \gamma = \sqrt{1 - (\lambda f_x)^2 + (\lambda f_y)^2} \quad (2.43)$$

We therefore define the angular spectrum of plane waves of the disturbance $U(x, y; 0)$ as the function:

$$A\left(\frac{\alpha}{\lambda}, \frac{\beta}{\lambda}; 0\right) = \int \int_{-\infty}^{\infty} U(x, y; 0) e^{-j2\pi(\frac{\alpha}{\lambda}x + \frac{\beta}{\lambda}y)} dx dy \quad (2.44)$$

After a prorogation of z the disturbance $U(x, y; z)$ can be written in form of angular spectrum like we did in equation 2.37:

$$U(x, y; z) = \int \int_{-\infty}^{\infty} A(f_x, f_y; z) e^{j2\pi(f_x x + f_y y)} df_x df_y \quad (2.45)$$

where $f_x = \alpha/\lambda$ and $f_y = \beta/\lambda$. To be a propagative disturbance, equation 2.45 should satisfy Helmholtz equation 2.20:

$$(\nabla^2 + k^2)U = 0 \quad (2.46)$$

Substituting equation 2.45 into 2.46 we have a differential equation:

$$\frac{d^2}{dz^2} A(f_x, f_y, z) + \left(\frac{2\pi}{\lambda} \right) [1 - (\lambda f_x)^2 + (\lambda f_y)^2] A(f_x, f_y, z) = 0 \quad (2.47)$$

A solution o this differenzial equation is:

$$A(f_x, f_y, z) = A(f_x, f_y, 0) e^{j \frac{2\pi}{\lambda} \sqrt{1 - (\lambda f_x)^2 + (\lambda f_y)^2}} \quad (2.48)$$

The propagative solution is the one where:

$$(\lambda f_x)^2 + (\lambda f_y)^2 > 1 \quad (2.49)$$

in this case the exponential into 2.48 remains complex and the wave can propagate. For the values of spatial frequencies that satisfy the condition:

$$(\lambda f_x)^2 + (\lambda f_y)^2 < 1 \quad (2.50)$$

the exponential in the equation 2.48 becomes real, and the wave resultant in not any more propagative since its exponential becomes a decay exponential. These waves are called evanescent waves. It is interesting to see how the angular spectrum theory is more complete than the Fresnel approximation

2.4. OPERATOR FREE SPACE PROPAGATION: ANGULAR SPECTRUM OF PLANE WAVES A

since includes evanescent waves too, very important in near field applications. Finally, the disturbance after a propagation in z can be expressed as a function of the disturbance $U(x, y; 0)$ at the plane $z=0$:

$$U(x, y; z) = \int \int_{-\infty}^{\infty} A(f_x, f_y, 0) e^{j \frac{2\pi}{\lambda} \sqrt{1 - (\lambda f_x)^2 - (\lambda f_y)^2}} e^{j 2\pi (f_x x + f_y y)} df_x df_y \quad (2.51)$$

The last equation looks very complex, but permits to calculate the output field $U(x, y; z)$ known the Input field and the propagation distance, under the approximation of propagation taking place in a linear, isotropic, homogeneous and non dispersive medium. Because of the linearity of the problem, we can consider the propagation as a linear system that maps the input disturbance $U(x, y; 0)$ into the a new field distribution $U(x, y; z)$. This linear system is characterized by a transfer function. The bandwidth of this transfer function is limited to the case of the propagative solution of equation 2.47, excluding the evanescent waves. We can rewrite the angular spectrum of the output field as the product of the angular spectrum of the input field multiplied by the transfer function $H(f_x, f_y)$: function of the disturbance $U(x, y; 0)$ at the plane $z=0$:

$$A(f_x, f_y; z) = A(f_x, f_y; 0) \cdot H(f_x, f_y) \quad (2.52)$$

The propagation is fully described by the transfer function:

$$H(f_x, f_y) = \begin{cases} e^{j \frac{2\pi z}{\lambda} \sqrt{1 - (\lambda f_x)^2 - (\lambda f_y)^2}} & \text{if } \sqrt{f_x^2 + f_y^2} < \frac{1}{\lambda} \\ 0 & \text{otherwise} \end{cases} \quad (2.53)$$

The propagation is therefore a linear band pass filter. The bandwidth can be represented as a circle in Fourier space. For frequencies smaller than $1/\lambda$ the transfer function introduces a shift in the spatial domain that in the end

gives the effect of the diffraction. Results obtained with the angular spectrum method are similar to the ones obtained with the Fresnel approximation, but no scaling factor between the input and output field is introduced. From a computational point of view, the angular spectrum operator is composed by 3 steps:

1. Fourier transform of the input field
2. Multiplication of the Fourier transform of the input field with the propagation transfer function in equation 2.53
3. Inverse Fourier transform of the product at step 2. The resultant field is the output disturbance after the propagation in free space.

The process can be seen in figure 2.3

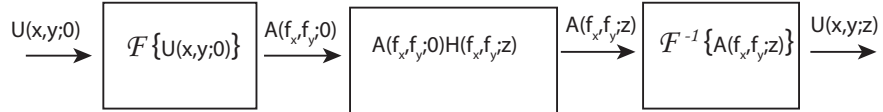


Figure 2.3: Structure of the operator free space propagation with the angular spectrum of plane waves method. The initial disturbance $U(x, y; 0)$ is transformed into the angular spectrum $A(f_x, f_y; 0)$ with a Fourier transform implemented by a FFT algorithm. The angular spectrum is multiplied by the propagation transfer function $H(f_x, f_y)$ and the resultant angular spectrum is inverse transformed into the output disturbance $U(x, y; z)$

2.4.2 Band Limited Angular Spectrum

The transfer function of the propagation shown in equation 2.53 is a complex exponential. Therefore is an oscillating function, whose frequency depends by the propagation distance z . In figure 2.4 are shown three different profile

Figure 2.4: example

of the transfer function for three different propagation distances. We can rewrite the transfer function as:

$$H(f_x, f_y) = e^{j\phi(f_x, f_y)} \quad (2.54)$$

where we indicated with ϕ the oscillating phase of the transfer function, such as:

$$\phi(f_x, f_y) = \frac{2\pi}{\lambda} \sqrt{1 - \lambda f_x^2 - \lambda f_y^2} \quad (2.55)$$

We can define the local spatial frequencies of the transfer function ν_x and ν_y along f_x and f_y the quantities:

$$\begin{cases} \nu_x = \frac{1}{2\pi} \frac{\partial}{\partial f_x} \phi(f_x, f_y) \\ \nu_y = \frac{1}{2\pi} \frac{\partial}{\partial f_y} \phi(f_x, f_y) \end{cases} \quad (2.56)$$

Therefore the local spatial frequencies are:

$$\begin{cases} \nu_x = -\frac{z}{\lambda} \frac{\lambda^2 f_x}{\sqrt{1 - (\lambda f_x)^2}} \\ \nu_y = -\frac{z}{\lambda} \frac{\lambda^2 f_y}{\sqrt{1 - (\lambda f_y)^2}} \end{cases} \quad (2.57)$$

If the input optical disturbance is sampled by and $N \times N$ sampling window with pixel size dx the transfer function is sampled by unit of spatial frequencies equals to $df = 1/(Ndx)$. To satisfy Nyquist condition in order to avoid aliasing the sample frequency should be at least the double of the bandwidth of the Transfer function. For one direction in the local frequency space:

$$\frac{1}{df} \geq 2|\nu_x| \quad (2.58)$$

Since modifying the sampling interval of the transfer function, and therefore of the input field, can lead to huge sampling windows and long computational times, in practical applications the sampling interval is fixed. This fact leads to a condition on the maximum frequency range for which the transfer function is not aliased:

$$\frac{1}{df_x} \geq 2z \frac{|f_x|}{|\sqrt{\frac{1}{\lambda^2} + f_x^2}|} \quad (2.59)$$

Resolving the equation for $|f_x|$ we have:

$$|f_x| \leq \frac{1}{\sqrt{(2df_x z)^2 + 1/\lambda}} = f_{max} \quad (2.60)$$

Where f_{max} is the maximum frequency of the transfer function without generating errors due to aliasing. Assuming the sampling of the optical field to be the same in both x and y direction, we can apply the same procedure to find out that the maximum bandwidth for the sampling in f_y is equal to the bandwidth in f_x . we get to:

$$\frac{1}{df_y} \geq 2|\nu_y| \quad (2.61)$$

$$\frac{1}{df_y} \geq 2z \frac{|f_y|}{|\sqrt{\frac{1}{\lambda^2} + f_y^2}|} \quad (2.62)$$

$$|f_y| \leq \frac{1}{\sqrt{(2df_y z)^2 + 1/\lambda}} = f_{max} \quad (2.63)$$

To avoid aliasing then, the two dimensional transfer function should be limited to a range of frequencies defined by 2.62. The expression of the output field will then be:

$$U(x, y; z) = \mathcal{F}^{-1} [A(f_x, f_y; 0) H'(f_x, f_y; z)] \quad (2.64)$$

2.4. OPERATOR FREE SPACE PROPAGATION: ANGULAR SPECTRUM OF PLANE WAVES A

where

$$H_{BL}(f_x, f_y; z) = H(f_x, f_y; z) \text{rect} \left(\frac{f_x}{f_{min}} \right) \text{rect} \left(\frac{f_y}{f_{min}} \right) \quad (2.65)$$

In the MATLAB algorithm the band limitation has been implemented multiplying the propagation transfer function by a to a circle function of radius f_{max} in the plane of the spatial frequencies. The resultant phase of the transfer function is shown in figure 2.5. From a computational point of view

Figure 2.5: example

the algorithm to implement the band limited angular spectrum method can be summarized in the following steps:

1. Computation of the angular spectrum of the input disturbance via a Fourier transform
2. estimation of the maximum bandwidth of the transfer function in order to avoid aliasing error
3. Multiplication of the angular spectrum for the band limited transfer function
4. Inverse Fourier transform of the product at step 3

The structure of the operator free space propagation implemented by the band limited angular spectrum can be seen in figure 2.6

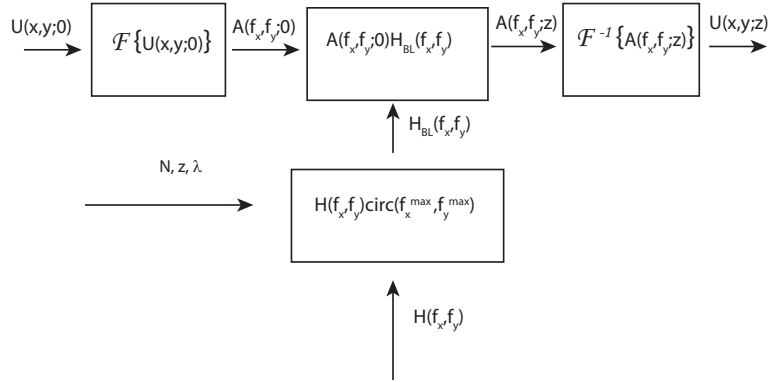


Figure 2.6: Structure of the operator free space propagation with the angular spectrum of plane waves method in its band limmited version. The initial disturbance $U(x, y; 0)$ is transformed into the angular spectrum $A(f_x, f_y; 0)$ with a Fourier transform implemented by a FFT algorithm. The angular spectrum is multiplied by the propagation transfer function $H(f_x, f_y)$ whose bandwidth has been limited according to equation 2.63. The bandwidth of the transfer function depends by the sampling of the input field, by the wavelength of the light λ and of course by the propagation distance. The resultant angular spectrum is inverse transformed into the output disturbance $U(x, y; z)$

2.4.3 Corrected Band Limited Angular Spectrum Method

Another issue is the fact that for long propagation distances the bandwidth of the transfer function might act a a low pass filter on the input field in case the maximum frequency of the signal is bigger than the cut-off frequency of the band limited method causing lose of resolutions in the final image. A trade-off should therefore be find between the error due to the aliasing and the error due to the excessive band limitation. For imaging application this simulation platform was designed for this is not an issue since the numerical aperture of the optical elements in the imaging system give already a limitation in the band passing from the input field to the out field. However it is useful to estimate the bandwidth of the propagation free space propagation defining

2.4. OPERATOR FREE SPACE PROPAGATION: ANGULAR SPECTRUM OF PLANE WAVES A

the maximum spatial frequency that is transferred to the object plane. With reference to figure 2.7 the spatial frequencies from a point in the input field that are transferred to the output field are the ones whose director cosines are contained into the angle that includes the sampling window of the output field. If the propagation distance is much bigger than the sampling window, this is the case of most of the application of this simulation toolbox, the angle θ is equal to:

$$\theta \simeq \frac{W}{z} \quad (2.66)$$

The link between the director cosine and the spatial frequency is, according

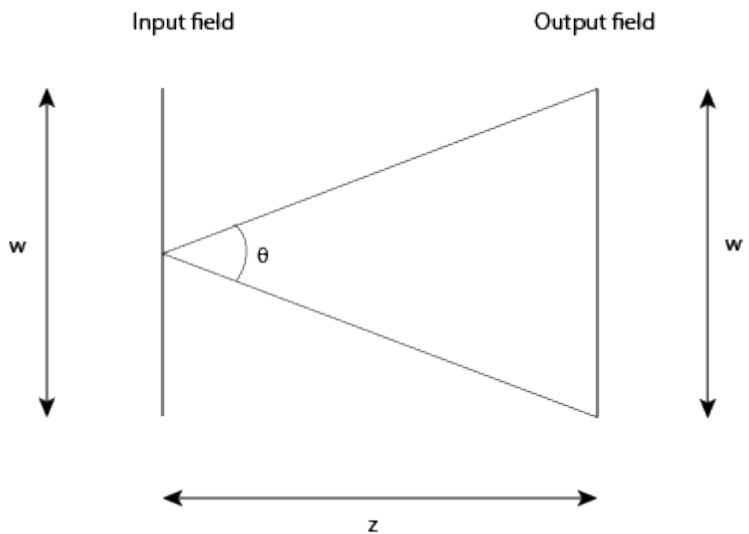


Figure 2.7: The maximum spatial frequency is linked to the dimension of the sampling window of the output field w and the propagation distance z

to equation 2.43

$$\theta = \lambda f_{cut-off}, \quad (2.67)$$

We then define the cut-off frequency of a field sampled by a sampling window that of W and after a propagation distance of z as:

$$\nu_{cutoff} = \frac{W}{\lambda z} \quad (2.68)$$

Therefore the bandwidth of the transfer function should be bigger than ν_{cutoff} in order not to introduce error in the reconstruction of the diffraction pattern due to loss in resolution.

$$f_{max} \geq \nu_{cutoff} \quad (2.69)$$

In case the propagation distance limits too much the bandwidth of the output field, the transfer function can be improved increasing the sampling of the input field. This condition is equal to have a smaller pixel size. Dealing with bigger sampling windows however increases the computational effort. The Angular spectrum method in all its variants always requires two Fourier transform in each propagation. For this reason, and in cases in which the sampling of the input field cannot be changed, it is useful to use the corrected band limited method, which consists in stopping the bandwidth of the transfer function can be limited by the cut-off frequency of the propagation shown in equation 2.68. To evaluate the differences in resolution of the three variants of the angular spectrum methods, Normal Angular spectrum (AS), band limited angular spectrum (BL), and corrected band limited angular spectrum (corrected BL), we simulated the propagation of a field represented by a circular pupil of diameter 5 mm, sampled with a resolution of 3000 by 3000 pixels, in a sampling window of 1 cm. The propagation distances varied from 1 m to 10 m. results are shown in figure where the cross section of the diffraction patterns are shown. It is evident that although

2.4. OPERATOR FREE SPACE PROPAGATION: ANGULAR SPECTRUM OF PLANE WAVES A

the BL method gives smooth and nice diffraction patterns, the information is lost due to the excessive low pass filtering action on propagation transfer function that occur at large propagation distances. A comparison with the non band limited method (AS) can be seen in figure , where the noise due to aliasing in transfer function sampling affect the resolution of the diffraction pattern. A good compromise is found using as bandwidth of the transfer function the bandwidth of the propagation as shown in figure. If we see the behaviour of the signal to noise ratio of the diffraction patterns of a pupil taken ad different propagation distances for the three cases, figure 2.9, we see that the band limited angular spectrum method gives a better SNR, blue line. This is due to the excessive smoothing action that brings to the loss of resolution. On the other hand without any limitation of the band, green line, the noise become dominant for long propagation distances and the SNR approach the zero value. The best results in terms of resolution and noise reduction are given by the corrected method, red line, where the information on the diffraction is entirely kept. on the as shown in figure 2.8 as well.

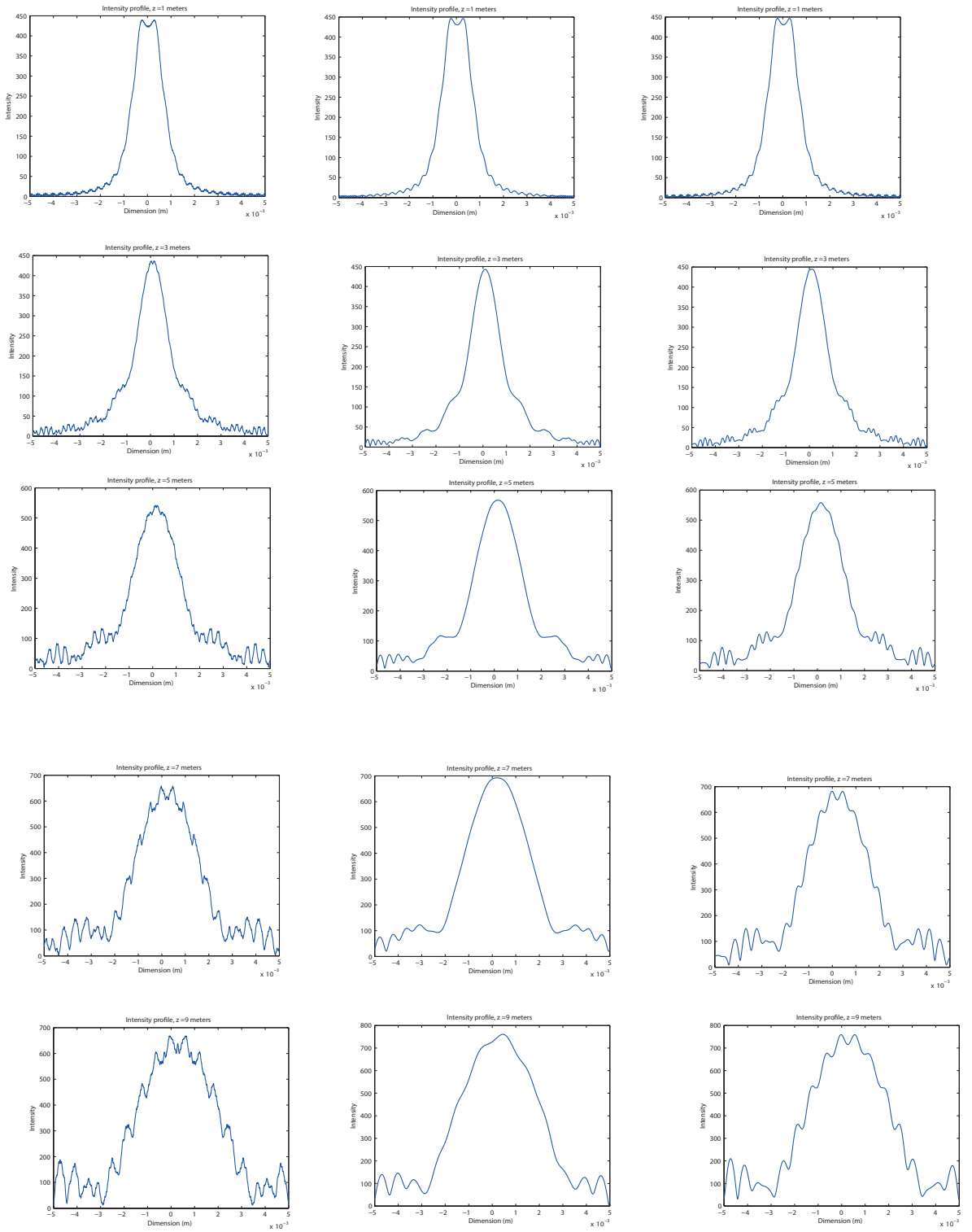


Figure 2.8: Comparison of the performances of the three angular spectrum propagation operator.

2.4. OPERATOR FREE SPACE PROPAGATION: ANGULAR SPECTRUM OF PLANE WAVES A

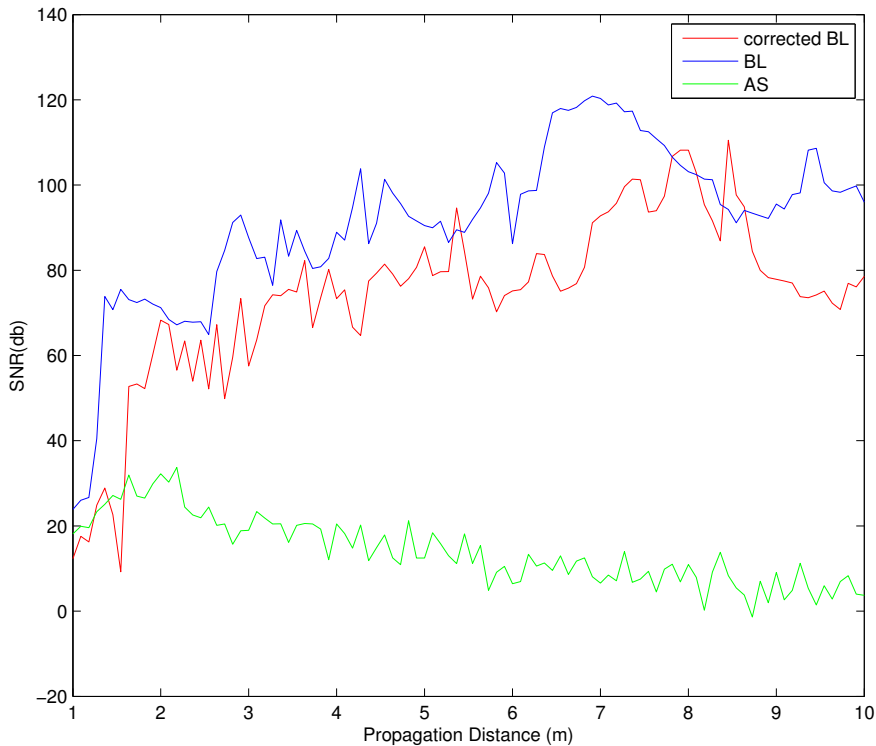


Figure 2.9: Comparison between the SNR as a function of the propagation distance for the three propagation method seen in section 2.4.1. The BL and the corrected BL methods improve the SNR, that instead drops with the increasing of the propagation distance when the normal AS method is used.

2.5 Operator Thin Lens

We consider a lens is composed of a material with a refractive index different from the refractive index of air, normally 1.5, in which the propagation velocity of the optical field is less than the propagation velocity air. In the approximation of a thin lens, the translation of the ray of light inside the lens is negligible and if a ray enters the lens at the coordinate (x, y) on one face, it exits at the same coordinates at the other side. A thin lens delays an incident wave front by an amount proportional to its thickness. This delays can be modelled introducing a phase factor to the incident field. We define a thickness function:

$$\Delta(x, y) \quad (2.70)$$

as the thickness of the lens at the coordinates (x, y) as shown in figure 2.10, where Δ_0 is the lens maximum thickness at the coordinates $(0, 0)$.

Figure 2.10: example

From the thickness function we can define the phase delay introduced by the lens as:

$$\phi(x, y) = kn\Delta(x, y) + k[\Delta_0 - \Delta(x, y)] \quad (2.71)$$

where n is the refractive index of the lens material. With reference to figure 2.10 $kn\Delta(x, y)$ is the phase delay introduced by the different material of the lens, and $k[\Delta_0 - \Delta(x, y)]$ is the phase delay introduced by the free space propagation between the two planes represented with dashed line. This phase

delay can be seen as a multiplicative phase term :

$$t_{lens} = \exp[jk\Delta_0] \exp[jk(n-1)\Delta(x, y)] \quad (2.72)$$

The complex field $U'(x, y)$ immediately after the lens is given by the product of the field entering the lens $U_0(x, y)$ with the phase delay in equation 2.72.

$$U'(x, y) = t_l(x, y)U_0(x, y) \quad (2.73)$$

Before carrying on with the derivation of the thin lens operator, we define a sign convention. For a ray of light travelling from left to right:

- any convex surface encountered has positive radius of curvature
- any concave surface encountered had negative radius of curvature

According to what is shown in figure 2.11 we split the lens into three elements such that the total thickness function is the sum of three functions: so that

Figure 2.11: example

we have:

$$\Delta(x, y) = \Delta_1(x, y) + \Delta_2(x, y) + \Delta_3(x, y) \quad (2.74)$$

Where

$$\Delta_1(x, y) = \Delta_01(x, y) - R_1 \left(1 - \sqrt{1 - \frac{x^2 + y^2}{R_1^2}}\right) \quad (2.75)$$

$$\Delta_2(x, y) = \Delta_02 \quad (2.76)$$

$$\Delta_3(x, y) = \Delta_03(x, y) - R_2 \left(1 - \sqrt{1 - \frac{x^2 + y^2}{R_2^2}}\right) \quad (2.77)$$

and $R_1 > 0$ and $R_2 < 0$ are respectively the radius of curvature of the right-hand surface and the radius of curvature of the left-hand side of the lens surface. Then the thickness function is given by:

$$\Delta(x, y) = \Delta_0(x, y) - R_1 \left(1 - \sqrt{1 - \frac{x^2 + y^2}{R_1^2}}\right) + R_2 \left(1 - \sqrt{1 - \frac{x^2 + y^2}{R_2^2}}\right) \quad (2.78)$$

where $\Delta_0 = \Delta_01 + \Delta_02 + \Delta_03$. If we consider a portion of the optical field close to the optical axis, the coordinates x and y are small, *paraxial approximation*, and the argument of the square root will be small as well, allowing us to approximate with its first element of the Taylor series:

$$\sqrt{1 - \frac{x^2 + y^2}{R_1^2}} \approx 1 - \frac{x^2 + y^2}{R_1^2} \quad (2.79)$$

$$\sqrt{1 - \frac{x^2 + y^2}{R_2^2}} \approx 1 - \frac{x^2 + y^2}{R_2^2} \quad (2.80)$$

The resulting phase transformation substituting 2.79 and 2.80 into equation 2.78 will only be valid under the paraxial approximation and can be written as:

$$\Delta(x, y) = \Delta_0(x, y) - \frac{x^2 + y^2}{2} \left(\frac{1}{R_1} + \frac{1}{R_2}\right) \quad (2.81)$$

If we substitute this equation 2.81 into equation 2.71 we get the expression of the phase shift in the exponential form:

$$t_l(x, y) = \exp[jkn\Delta_0] \exp[-jk(n-1) \frac{x^2 + y^2}{2} \left(\frac{1}{R_1} + \frac{1}{R_2}\right)] \quad (2.82)$$

We define now the focal length of the lens f , the quantity containing the information on the physical properties of the lens, as:

$$\frac{1}{f} \equiv (n-1) \left(\frac{1}{R_1} + \frac{1}{R_2}\right) \quad (2.83)$$

Finally after dropping the constant phase factor we can write the effect of a thin lens under par-axial approximation as a quadratic phase transformation:

$$t_l(x, y) = \exp[-j \frac{k}{2f} (x^2 + y^2)] \quad (2.84)$$

This equation can represent the effects of any lens, since the sign of f will define whether the lens is positive or negative. The physical meaning of this expression can be understood examining figure 2.12 When a plane wave,

Figure 2.12: example

represented by the complex field $U(x, y)$, is normally incident on the lens, according to equation 2.73, the field coming out of the lens will be:

$$U'(x, y) = \exp[-j \frac{k}{2f} (x^2 + y^2)] \quad (2.85)$$

The thin lens is introducing a phase term on the incident field, and the resulting field is a quadratic approximation of a spherical wave. As shown in figure 2.12 when f is positive, the wave is converging towards a point on the optical axis at distance f from the lens. If f is negative the wave is diverging from a point on the optical axis placed at a distance $|f|$ in front of the lens. The lens therefore transforms a plane wave into a spherical wave. We can now define the operator thin lens as the product of the quadratic transformation in equation 2.84 by a function describing the aperture of the lens, called pupil function $P(x, y)$:

$$L(x, y) = P(x, y) \exp[-j \frac{k}{2f} (x^2 + y^2)] \quad (2.86)$$

where the pupil function is defined as:

$$P(x, y) = \begin{cases} 1 & \sqrt{x^2 + y^2} < r \\ 0 & \text{elsewhere} \end{cases} \quad (2.87)$$

where r is the the radius of the lens aperture.

2.5.1 Aliasing in phase sampling

The quadratic phase factor of the thin lens operator is a complex function whose modulus is constant and equal to the unity, and its argument is an oscillating function in the interval $(0, 2\pi]$. The argument of the phase factor is shown in figure 2.13 Figure 2.13 shows how the parabolic phase profile

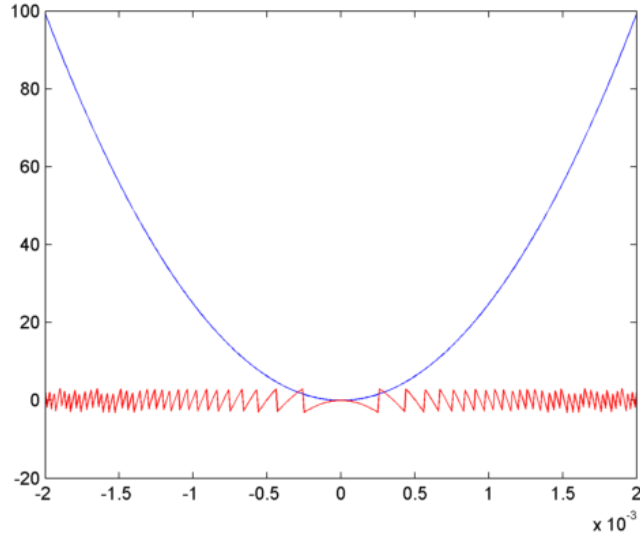


Figure 2.13: Phase profile of a computer generated lens. In Blue it is shown the unfolded quadratic phase term, in red the folded one, subject to aliasing.

when is in the form of the phase factor gets wrapped since the argument of a complex function varies between 0 and 2π . This wrapping of the phase can cause problem of aliasing as the distance from the centre of the lens increases. For high values of x and y , the quadratic term became too steep

and the frequency of oscillation between 0 and $2\pi f$ of the phase factor might became such that it is not any more correctly sampled. With analogy of what has been said in section 2.4, for the parabolic phase profile:

$$\Phi(x, y) = \frac{k}{2f}(x^2 + y^2) \quad (2.88)$$

we can define the instantaneous frequencies of the phase ν_x , ν_y in x and y respectively as:

$$\begin{cases} \nu_x = \frac{1}{2\pi} \frac{\partial \Phi}{\partial x} = \frac{1}{2\pi f} k x \\ \nu_y = \frac{1}{2\pi} \frac{\partial \Phi}{\partial y} = \frac{1}{2\pi f} k y \end{cases} \quad (2.89)$$

In order to recover all the components of a periodic signal, the sampling frequency should be at least twice the maximum frequency contained into the signal. The Nyquist frequency is:

$$f_{Nyquist} = 2\nu_{max} \quad (2.90)$$

The maximum instantaneous frequency of the phase factor in the operator thin lens happens in correspondence with the maximum value of the spatial coordinate of the lens. We consider for brevity the one dimensional case along the x direction, but the conclusions are valid for the y direction because of the definition of pupil function in equation 2.87. In this case $x_{max} = y_{max} = r$ where r is the radius of the pupil function. Defining the pixel size Δx along x , and assuming the pixels as squared, so that the sampling frequency $\frac{1}{\Delta x}$ is the same along both axis the condition to avoid aliasing is according to Nyquist criterion:

$$\frac{1}{\Delta x} \geq \frac{1}{2\pi f} k x_{max} \quad (2.91)$$

Since in general the sampling rate, cannot be modified because of the fixed pixel size of the sensor this expression leads to a condition for the radius of the pupil function:

$$r = x_{max} \leq \frac{2\pi f}{k\Delta x} \quad (2.92)$$

Substituting $k = \frac{2\pi}{\lambda}$ into 2.92, we have:

$$r \leq \frac{\lambda f}{\Delta x} \quad (2.93)$$

The more powerful is the lens, small values of f , the smallest should be the aperture of the pupil function. Since the simulation platform is flexible, in case a particular aperture is needed, we can modify equation 2.93, in order to get a condition on the focal length:

$$f \geq \frac{\Delta x r}{\lambda} \quad (2.94)$$

And considering that the resolution of a with aperture equal to $2r$ the lens is given by:

$$N = \frac{2r}{\Delta x} \quad (2.95)$$

The minimum resolution of a lens of radius r and focal length f is:

$$N \geq \frac{2r^2}{f\lambda} \quad (2.96)$$

$$\left\{ \begin{array}{l} \nu_x = \frac{\partial \Phi}{\partial x} = \frac{1}{\lambda f} x \\ \nu_y = \frac{\partial \Phi}{\partial y} = \frac{1}{\lambda f} y \end{array} \right. \quad (2.97)$$

2.6 Comparison between the free space propagation operators

In this section we analyse the difference in performance between the Fresnel approximation and the angular spectrum of plane waves approach, with particular attention to the computational time required by the different methods,

the optical resolution and the error. Having defined the operator thin lens we can simulate the first simple imaging system. Results will be used to evaluate the characteristic of the different propagation operators.

2.6.1 Description of the system

The system simulated is a simple imaging system composed by a single lens with focal length $f = 158mm$, in a 2f configuration, as shown in figure 2.14. The field of view is a square of 1cm by 1cm, sampled by a sampling window of 2000 by 2000 pixels. The aperture of the lens is $D = 5mm$ and its f number, defined as:

$$F_{num} = \frac{z}{D} \quad (2.98)$$

is equal to $F_{num} = 63$, where z is the distance from the lens to the image plane, that in a 2f configuration is equal to $z = 2f = 316mm$. The optical

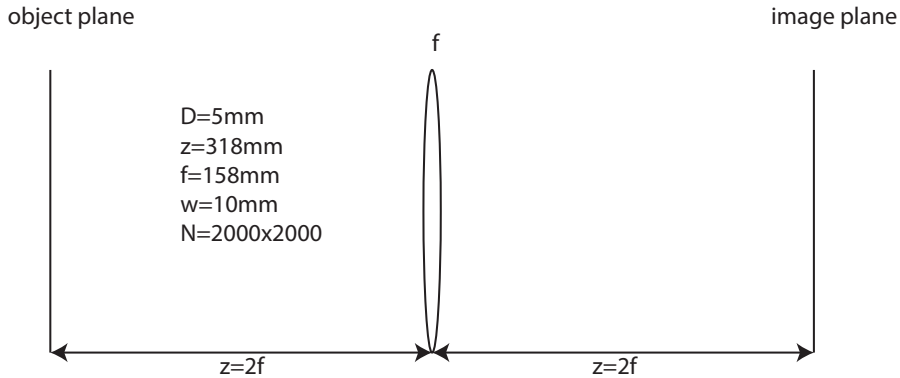


Figure 2.14: Schematic of the 2f system simulated. f is the focal length, z the propagation distances, D is the aperture of the lens, w the field of view and N the sampling resolution.

cut-off frequency of this system is given by the relation:

$$\nu_c = \frac{1}{\lambda F_{num}} \quad (2.99)$$

and for the system simulated, illuminated with monochromatic light with wavelength equal to $\lambda = 633nm$, we have $\nu_c = 2.5 \cdot 10^4 cycles/m$.

2.6.2 Image of a point source

The first experiment simulated is the image of a point source, rendered with a pinhole of $10\mu m$ of diameter placed at the object plane indicated in figure 2.14. The image has been taken using four different methods to propagate the light into the system. Those are:

- Multi step Fresnel method (MSF)2.3.1
- Angular spectrum method (AS)2.4
- Band Limited Angular Spectrum method (BL)2.4.1
- corrected Band Limited Angular Spectrum method (cBL) 2.4.3

The image of a point source is a useful method to analyse the impulse response of the optical system simulated, as well as of the sequence of the single operators used. the sequence of the operator is illustrated in figure 2.15 the

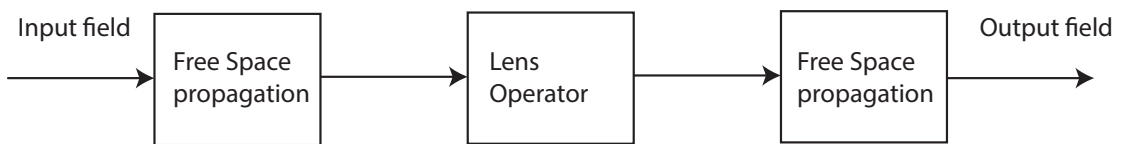


Figure 2.15: Operator sequence for the 2f system.

impulse response of an optical system is an Airy Disk, that is the Fourier transform of the pupil of the system at the image plane. The shape and the dimension of the central lobe of the Airy Disk give many information on

the characteristic of the optical system. The fact that the theoretical output of the experiment is well known allow us to determine the quality of the simulations tools. In addition to that, the Fourier transform of the impulse response of an optical system gives information on the frequencies contentn of the system and the quality of the system. In figure 2.16 are shown the sensor image at the image plane together with cross section intensity profile the image. It is evident from figure 2.16 that the band limited angular spectrum method reduce the noise due to aliasing of the transfer function. It also shown that the multi step method does not give a quantitative accurate result, since the noise the Airy disk, that never goes to zero. the reduction in noise can be seen also in an enhancement of the contrast in the images when passing from the multi step to the angular spectrum methods. the contrast is even better when the band limited method is used. From these results comes also a validation of the simulation platform. The Airy disk first minimum is at a position:

$$d = 1.22 \frac{\lambda z}{D} \quad (2.100)$$

where λ is the wavelength of the light propagating, D is the aperture of the lens and z the propagation distance. According to the values in section 2.6.1 the Airy disk should have a width of $d = 67\mu m$. Without considering the multi step case that is too noisy to find a minimum, the position of the first minimum is the other cases are:

AS	$67.5 \mu m$
BL	$77.5 \mu m$
cBL	$77.5 \mu m$

As expected for the band limited angular spectrum the Airy Disk is slightly wider due to the low pass filtering action that transfer function has undergone. However noise is reduced sensibly with the band limitation. 2.16.

2.6.3 Frequency analysis

To better understand how the resolution changes with the different methods, we have a look at the Fourier transform of the images shown in figure 2.16. Results are shown in figure 2.17. The graphs are symmetric respect to the zero frequency.

2.6. COMPARISON BETWEEN THE FREE SPACE PROPAGATION OPERATORS 63

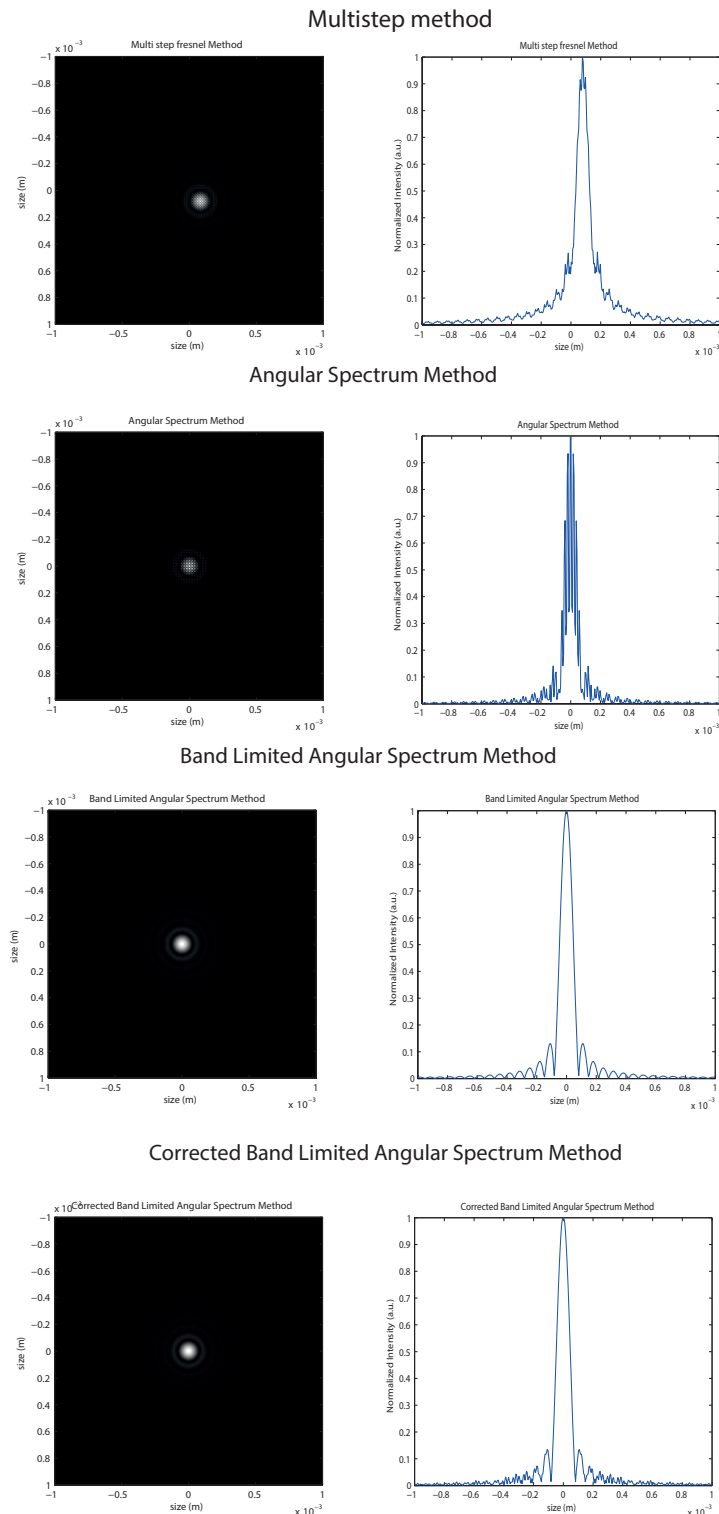


Figure 2.16: From top to Bottom: Image and intensity cross section of a point source according to multi step method, angular spectrum method, band limited angular spectrum method and corrected band limited angular spectrum method.

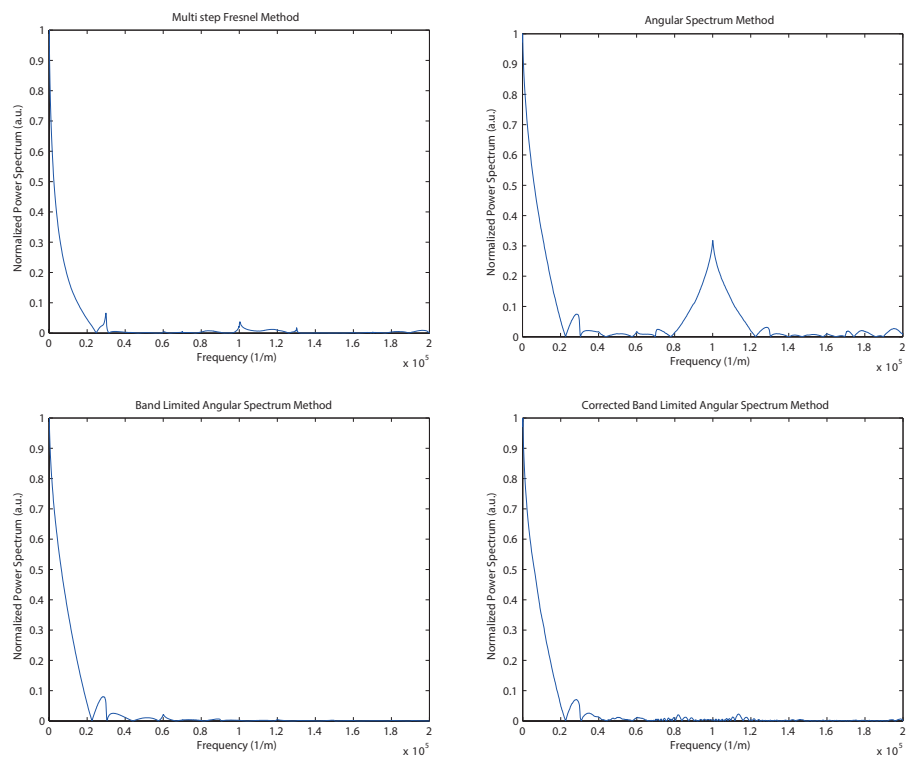


Figure 2.17: From top left to bottom right: Power spectrum of the image of a point source obtained with the multi step Fresnel method, the Angular spectrum method, the band limited angular spectrum method and the corrected band limited angular spectrum method .

2.7 Coherence

The Fresnel simulation toolbox has been designed to analyse a light field imaging system. As discussed in section in order to avoid loss of information because of the interference effect and fringes across lens lets, we decided to develop a system that used low coherence light. In addition to that, the reconstruction algorithms explained in section require a large number of details in the field of view, and incoherent illumination allows to detect better edges and features in a scene, as explained by Goodman. We need therefore develop a way to simulate light in any state of coherence. So far we dealt with have analysed with diffraction, that is a deterministic property of light. Once the characteristics of the input complex optical field are known, we have seen methods that permit to determine the characteristics of the output complex optical field completely. 2.32.4.12.4

We now shift our attention to another property of light that is not deterministic, and therefore can only be described under a statistical point of view. The statistical properties of light have an important role in determining the output complex field in an imaging system. Coherence is one of this statistical properties and is described in terms of second order averages known as coherence function. A full analysis of coherence of optical fields can be found in text books such as Born and Wolf [3] and Goodman [7]. For our applications we will treat coherence under a less rigorous point of view, focusing on the practical effects on the optical experiments, and on elaborating and algorithm to simulate different levels of coherence. Before analysing the computational side of coherence it is worth to define what the two types of

coherence as defined by Goodman [7]:

- **Temporal Coherence** can be defined as the ability of light to interfere with a delayed version of itself
- **Spatial Coherence** can be defined as the ability of light to interfere with a spatially shifted version of itself

We developed an empirical method to simulate light propagating at different degree of coherence both spatial and temporal in order to investigate the dependence of the optical system from the coherence degree of light. in our software both types of coherence will be simulated at the same time producing a low coherent light source.

2.7.1 Temporal coherence

As following the explanation of Goodman [7], given a complex disturbance $U(\vec{X}, t)$ with a finite bandwidth $\Delta\nu$, it is expected to remain constant during a time interval $\tau < 1/\Delta\nu$. This means that the disturbance taken at two different times in the same spatial position $U(\vec{X}, t)$ and $U(\vec{X}, t + \tau)$ are highly correlated if $\tau < \tau_c$ where $\tau_c = 1/\Delta\nu$ is the coherence time. Since the correlation takes place without any spatial shift it is possible to drop the spatial coordinates \vec{X} . The degree of temporal coherence is therefore given by the autocorrelation function:

$$\Gamma(\tau) = \langle U(t + \tau)U^*(t) \rangle \quad (2.101)$$

the coherence time is therefore a function of the bandwidth of the light. Perfectly monochromatic plane wave whose bandwidth is very narrow is therefore a long time of coherence. While laser pulses will have a coherence time

that is dependent by the bandwidth of the pulse. Usually the shortest is the pulse, the wider is the bandwidth. From the time of coherence it is possible to define the coherence length $l_c = v\tau_c$ where $v = c/n$ is the speed of light in the medium of propagation. c is the speed of light in the vacuum and n the refractive index.

2.7.2 Spatial Coherence

To analyse spatial coherence we consider two complex disturbances $U(\vec{X}_1, t)$ and $U(\vec{X}_2, t)$ taken at the same time in two different position \vec{X}_1 and \vec{X}_2 . When the two points coincide, $\vec{X}_1 = \vec{X}_2$ the two disturbances are perfectly correlated. When the distance between the two points begin to increase, the correlation degree decreases until they become uncorrelated. The light source has a limited spatial coherence. In order to better understand spatial coherence it is useful to illustrate the Young experiment [15]. With reference to figure given a squared light source of size Δx emits light towards a screen at a distance. It is possible to define as area of coherence the σ_c as the area on a TO BE CONTINUED The spatial coherence gives an idea of the phase profile of the light source.

2.7.3 Simulation of spatial coherence

This method is based on the origin of light emitted by a source and as far as we know is totally new. It allows to generate a light source with a degree of coherence defined by the user. An electromagnetic wave is generated by a dipole oscillating at a certain frequency. This dipole can be a molecule, an atom, a group of atoms in a gas. In case of a conventional incandescence light

source light is emitted by tungsten atoms excited by the electrical current. Same is valid for other sources of illuminations, like gas lamps, neon, or solid state light sources like LED. Each dipole emits light with a certain initial phase. If we consider a light source of surface Σ , containing oscillating dipoles, we can identify elemental surfaces $d\Sigma$ as the surfaces on which all the dipoles oscillates with the same phase. The average dimension of the elemental surfaces $d\Sigma$ is proportional to the degree of spatial coherence of the light source. The more coherent is the light source, the bigger the elemental surfaces will be. From a computational point of view having a light source composed by a mosaic of surfaces with different phases is equivalent to add a phase mask to the input field. The phase mask is composed by areas with a random phase value. The dimension of these areas gives an idea of the degree of spatial coherence. The idea behind the empirical method used to generate the phase mask is shown in figure 2.18:

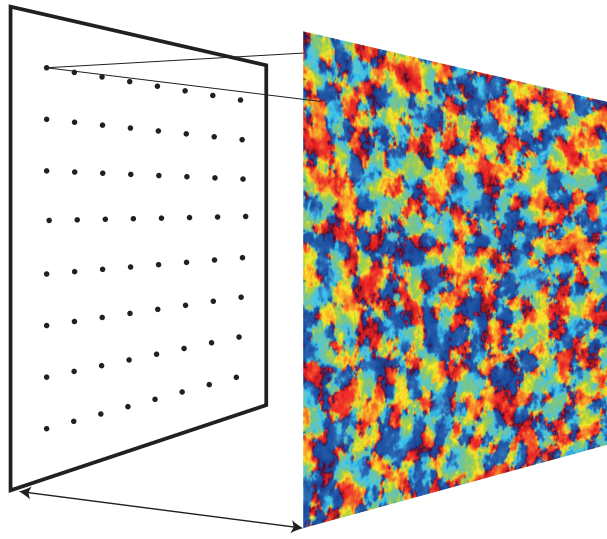


Figure 2.18: A random phase mask is generated propagating light coming from an array of sources, each one with a random phase value in the interval $[-\pi, \pi]$.

An array of point sources is displaced on a sampling window of the same dimension as the input field. The sources are placed regularly across the array. If the number of sources is less than 20, the sources are displaced randomly in order not to affect the coherence with their regular structure. The number of point sources used is given by the coherence index C . To each of these point sources is assigned a random value of phase in the range $[-\pi, \pi]$ and an amplitude value of one. Then a convolution kernel K is defined in order to make all the random point sources to merge together. The size of the kernel depends on the resolution N of the input field and on the coherence index C and is equal to the ratio N/C . After convolving the kernel K with the array of point sources we have a phase mask that is formed by an array of circular areas with a random phase value. Although this array of sources is already a phase mask, it cannot be used into the simulation platform,

because of its periodicity. In fact it is not a random phase pattern. In order to randomize the shape and the distribution of the coherence areas the array of sources is propagated at a distance bigger than the size of the sources. The distance chosen to propagate the light sources is the one that we derived in 2.3.1 to keep the same sampling both in the input and output fields using the Fresnel propagation method exposed in section. From equation 2.34 we have:

$$d_c = \frac{W^2}{N\lambda} \quad (2.102)$$

where W is the field of view, N is the sampling and λ is the wavelength of the light. The choice of using the Fresnel propagation as described in section 2.3 has been made because the propagation distance is not so big to give aliasing problem, and because it requires only one Fourier transform, making the random phase generation algorithm faster. the whole process is shown in figure 2.19 Few examples of phase mask generated from different number of sources can be seen in figure 2.20: To recap the algorithm to generate the random phase mask has the following steps:

- A number of light sources, depending on coherence index C , are defined and arranged in a regular array, and allocated a random phase between $-\pi$ and π .
- Each source has a size diameter given by: N/C
- This array of sources is then propagated a distance d_c shown in equation 2.102 in order to randomize the shape of the coherence areas.
- the resultant phase is used as the output phase mask to add the input

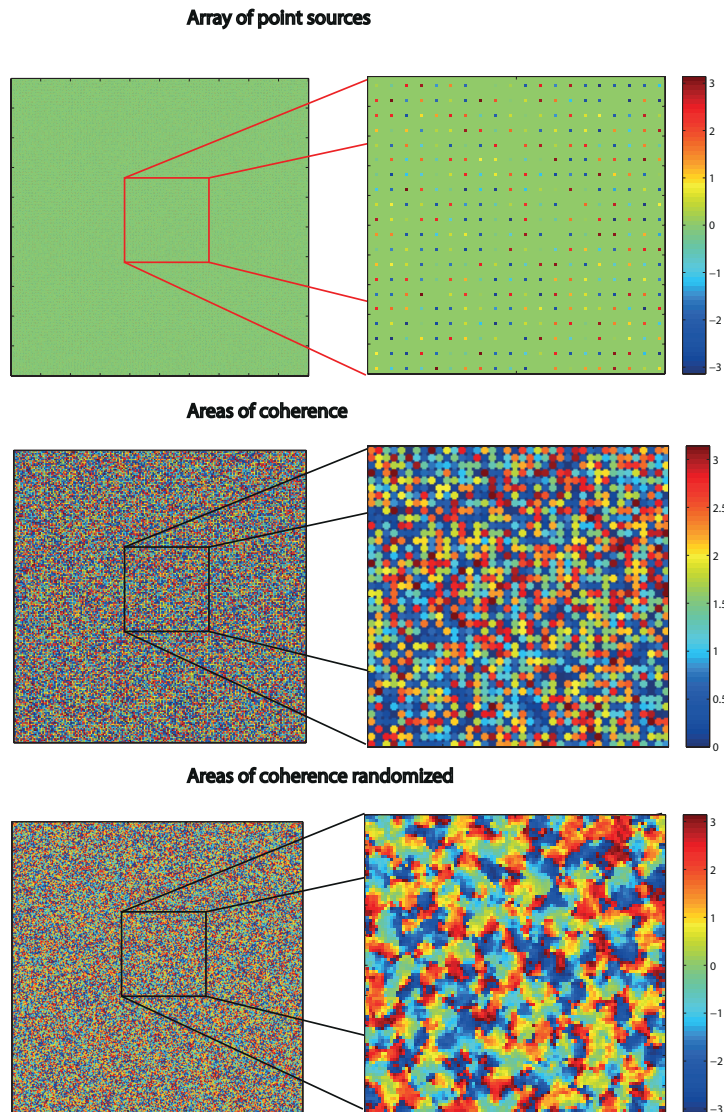


Figure 2.19: Process of the creation of the phase mask. Top: array of point sources with a random phase value; centre: array of the areas of coherence after the convolution with K ; bottom: randomized areas of coherence after the propagation of d_c .

field.

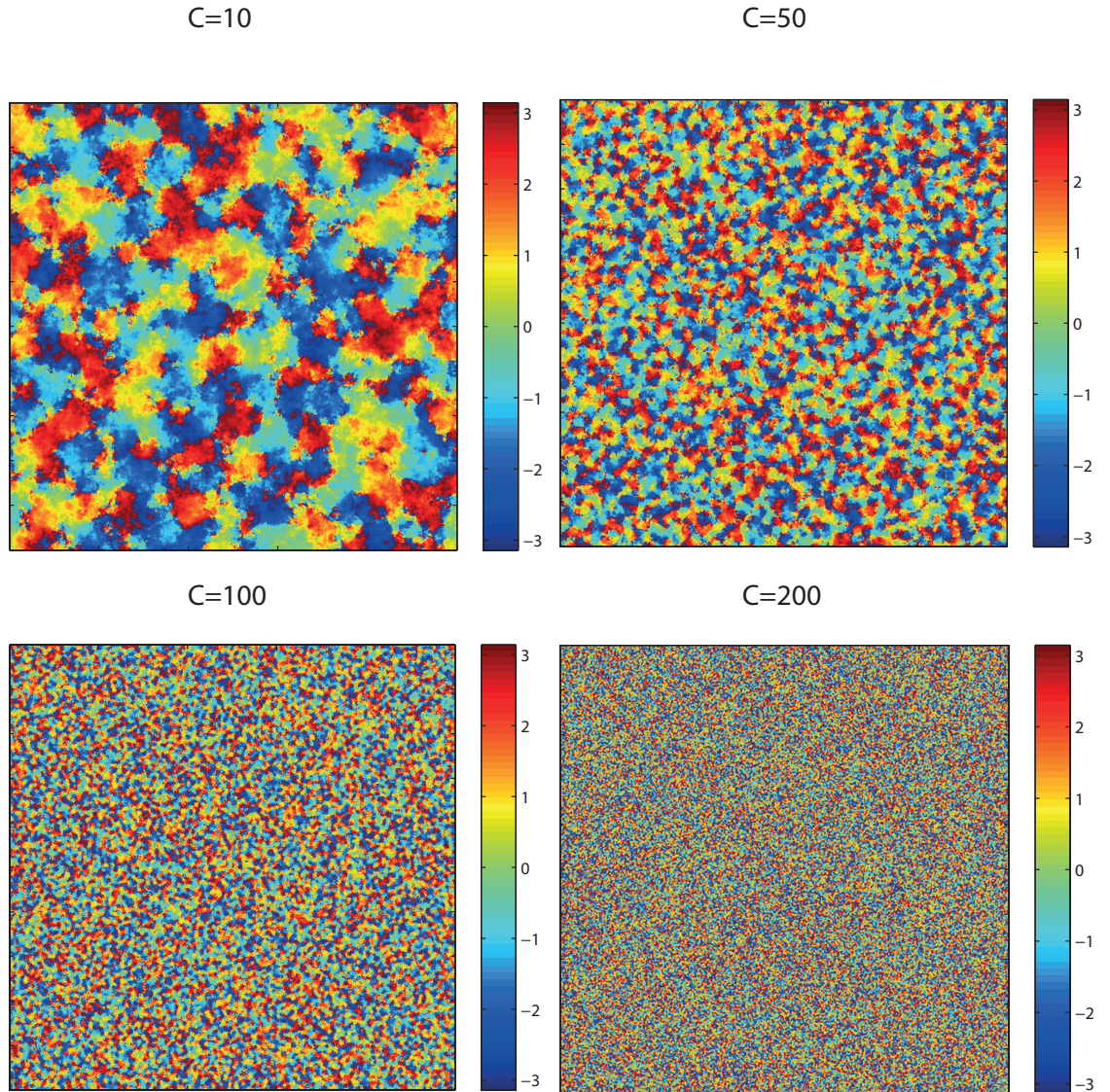


Figure 2.20: Final random phase mask generated by 10, 50, 100 and 200 sources.

2.7.4 Simulation of temporal coherence

Along with spatial coherence there is temporal coherence. temporal coherence is defined as the time τ in which the optical wave is correlated with itself. In other words after a time $t = \tau$, the optical disturbance $U(t)$ and

$U(t + \tau)$ are totally uncorrelated and cannot interfere with each other. To simulate this effect we have take many snapshots of the output field changing every time the phase mask described in section 2.7.3. We assume that the time difference between every snapshots is equal to the coherence time τ . For the application for which this toolbox has been designed it is not relevant to know the exact value of τ . However, the light source used for the real system was a "Thorlabs LED Array Light Source LIU630A", with a wavelength centred on 630 nm and a bandwidth $\Delta\lambda = 20nm$. The emission spectrum is shown in figure

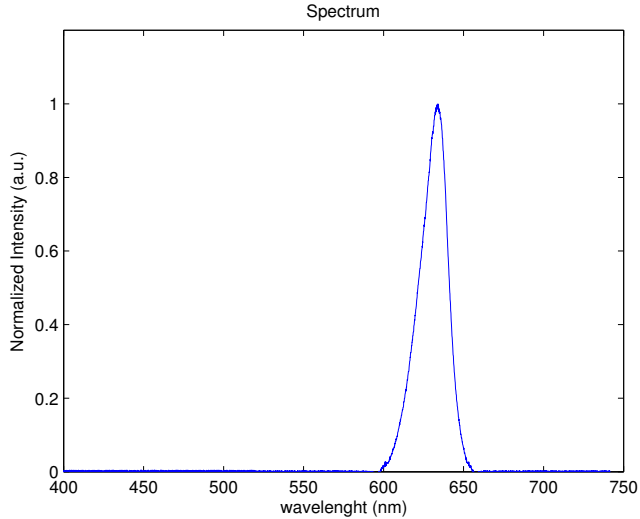


Figure 2.21: Emission spectrum of the LED considered in our simulations and real image system.

Its coherence time is given by:

$$\tau = \frac{1}{\Delta\nu} = \frac{\Delta\lambda}{c} \quad (2.103)$$

That gives a time of coherence $\tau = 6.6 \times 10^{17}s$. Therefore each snapshots is assumed to be taken at interval of τ . All the snapshots are then added

together, integrating the optical disturbance over time. The number of snapshots gives affects the quality of the image. Longer integration times will give better contrast and less noise as it is shown in the following paragraph.

2.8 Optimization of coherence parameters

In the previous paragraphs we have seen how to simulate partially coherent light and how to implement an algorithm that produces a certain number of snapshots of the output field each one with a different random phase. The random phase mask simulates the spatial coherence, the number of iteration instead simulates the effects of temporal coherence.

2.8.1 Optimization of Spatial Coherence

To define the optimal parameters to have a good image we have run simulations changing first the coherence index C , and evaluating the signal to noise ratio of the outcome images from the 2f system shown in figure 2.14. The input field is the USAF resolution target, shown in 2.22

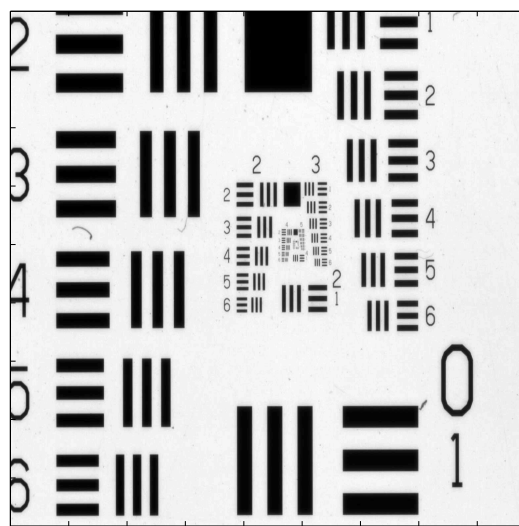


Figure 2.22: USAF resolution target.

The first simulation has been made changing the coherence index C from a value of 5 (high coherence) to 500 (low coherence) in a sampling window with a resolution of 1765 by 1765 pixels. Figure shows how the image field appears, while figure shows the signal to noise ratio of the images as a function of the coherence index. What catch attention is its asymptotic behaviour. After a certain threshold value of C , increasing the coherence index does not improve the image quality. The Threshold is defined as the value of C for which the variance of the previous five values of SNR is less than 0.01.

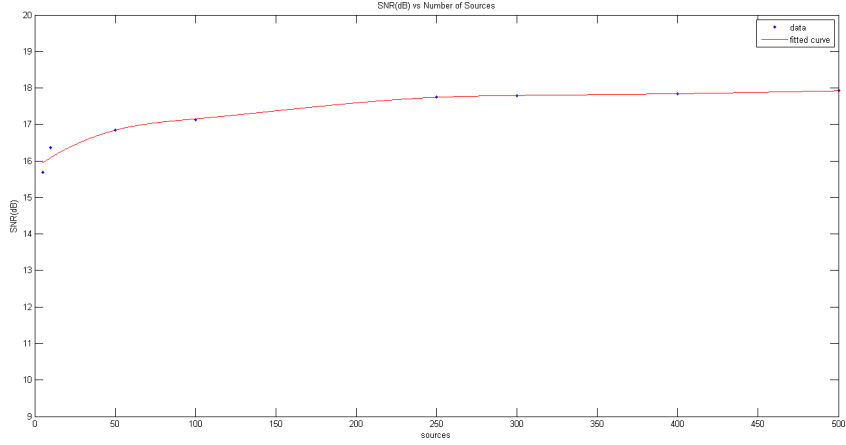


Figure 2.23: Signal to noise ratio of the image of a USAF resolution target plotted as a function of the coherence index C .

From figure 2.23 we see that for values of C bigger than 250 the SNR asymptotically tends to 18. Since the resolution of the input field, and therefore of the phase mask, is 1765 by 1765 pixels, we can conclude that the ratio between the number of sources and the resolution should be around 0.14. Increasing the number of sources does not improve enough the SNR, therefore there's no point in making the light source more incoherent. We can therefore define as incoherence degree a new parameter:

$$\iota = \frac{C}{N} \quad (2.104)$$

Acceptable results of incoherence are achieved for $\iota \sim 0.14$. Using the incoherence degree is better because it is not correlated to the sampling of the input field. In figure are shown the images of the target shown in figure 2.22 obtained with different incoherence parameters ι

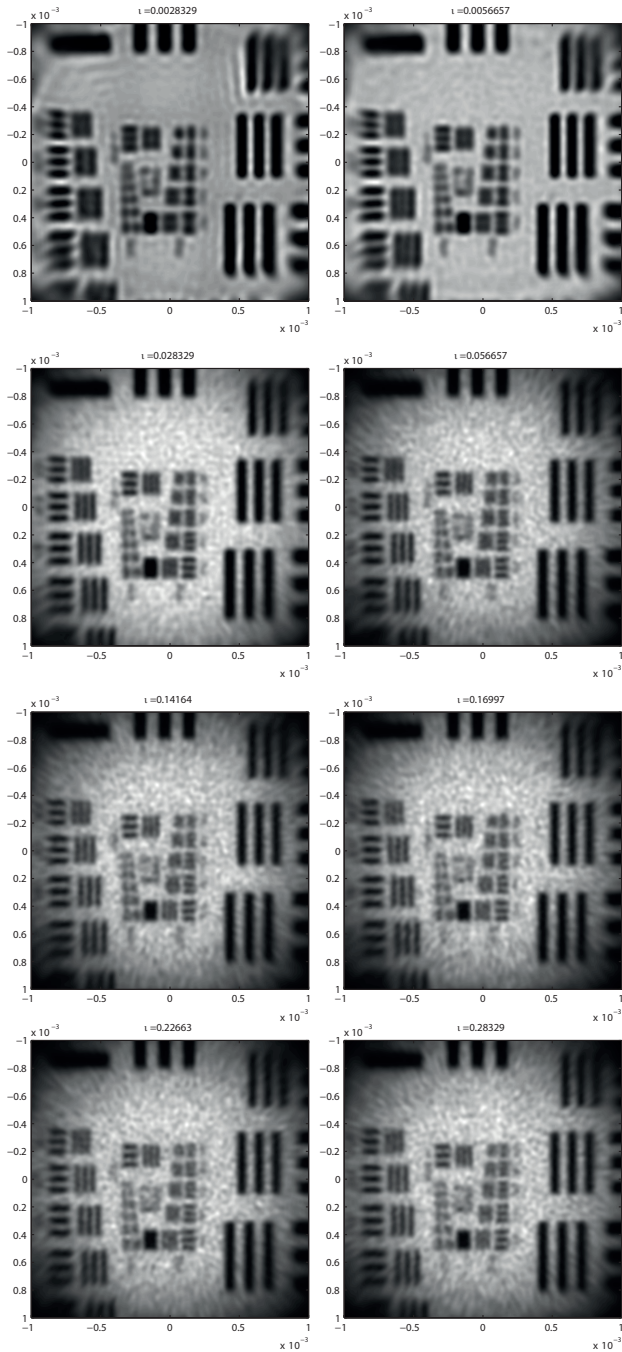


Figure 2.24: Images of the USAF resolution target with different values of ν . Increasing the number of point sources generating the phase mask creates improves the resolution and the contrast

2.8.2 Optimization of temporal coherence

The second simulation run aimed to define the optimum number of snapshots in order to correctly simulate temporal coherence. The random phase mask acts as a diffuser, and the resultant output field will present a low signal to noise ratio due to speckles, as shown in figure 2.25

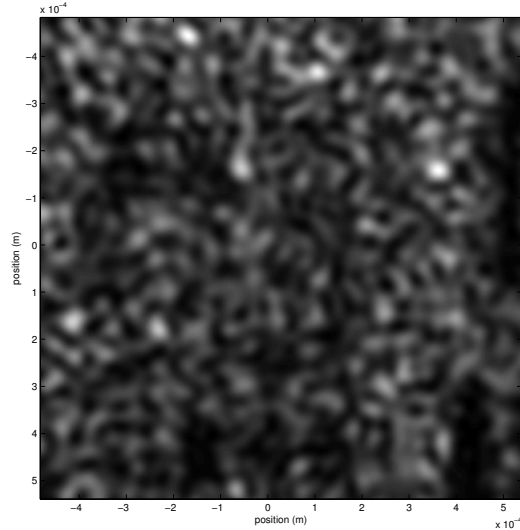


Figure 2.25: Noise due to the speckles ini an image of a USAF resolution target after only 5 iterations.

Taking several snapshots and adding them all together is equal to integrate over time the optical field reaching the sensor. While increasing the integration time, the noise due to the speckles drops considerably. In figure are shown several images of the USAF target in figure 2.22 taken with an incoherence degree of $\iota = 0.14$, and with an increasing number of iterations from 5 to 1000.



Figure 2.26: Images of the USAF resolution target obtained adding an increasing number of snapshot. this is equivalent to increase the integration time of the sensor. As an effect of that the noise due to the speckles caused by the phase mask decreases.

Since increasing the number of iteration is computationally expensive, the optimum number of iterations has been estimated evaluating the signal to noise ratio of the images in figure 2.26. results are shown in figure 2.27. The Threshold is defined as the number of iterations for which the variance of the previous five values of SNR is less than 0.01.

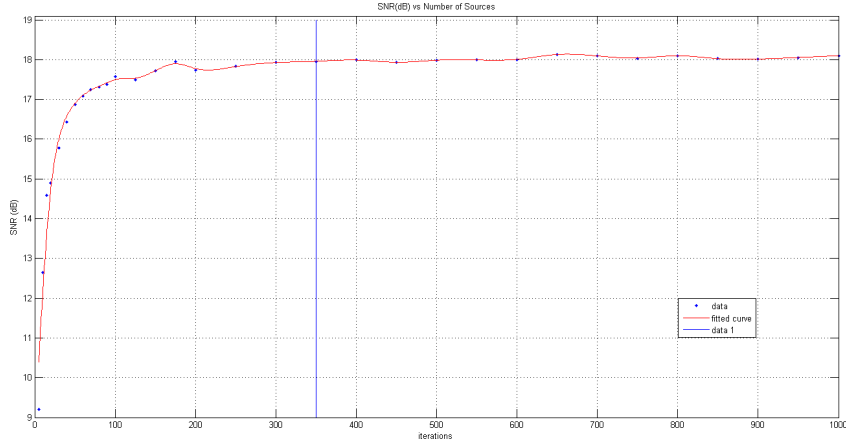


Figure 2.27: Signal to noise ratio as a function of the number of iterations. The threshold has been calculated looking at the variance of the previous five data.

For an image with an incoherence degree of $\iota = 0.14$ the minimum number of iterations that gives a good quality of the image is 350. After that value the SNR tends asymptotically to 18 dB, and in spite of an increased computational effort, we get no sensitive improvement in image quality

2.8.3 Coherent imaging vs incoherent imaging

To conclude, we simulated the image of an edge. The profile of an imaged edge is well known both in case of coherent and incoherent illumination and it presents some characteristics that allows to quantify how good how model

of incoherent propagation is. In figure 2.28 is shown the profile of an edge...

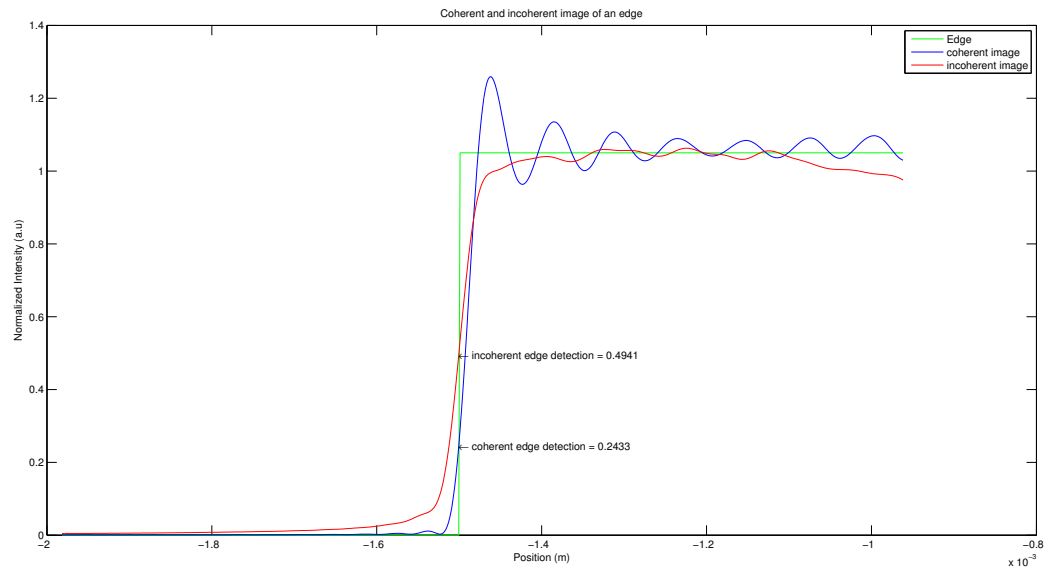


Figure 2.28: .

Chapter 3

Simulations of a plenoptic 1.0 system

3.1 Description of the system

3.2 Computer generated light fields

3.3 Rendering

3.4 Depth estimation

3.5 Tomography

3.6 Conclusion

Chapter 4

Simulation of a plenoptic 2.0 system

4.1 Description of the system

4.2 Optical performances of a focused plenoptic system

4.3 Optical resolution

4.3.1 Impulse response and OTF

4.3.2 Two point resolution

4.3.3 Optical cutoff frequency

4.4 Aberrations

Chapter 5

Light Field Microscope

- 5.1 Introduction**
- 5.2 optical setup**
- 5.3 Performances of the system**

Bibliography

- [1] Edward H Adelson and James R Bergen. *The plenoptic function and the elements of early vision*. Vision and Modeling Group, Media Laboratory, Massachusetts Institute of Technology, 1991.
- [2] Edward H Adelson and John Y. A. Wang. Single lens stereo with a plenoptic camera. *IEEE Transactions on Pattern Analysis & Machine Intelligence*, (2):99–106, 1992.
- [3] Max Born and Emil Wolf. *Principles of optics: electromagnetic theory of propagation, interference and diffraction of light*. Cambridge university press, 1999.
- [4] Todor Georgiev and Chintan Intwala. Light field camera design for integral view photography. *Adobe System, Inc*, 2006.
- [5] Todor Georgiev and Andrew Lumsdaine. Focused plenoptic camera and rendering. *Journal of Electronic Imaging*, 19(2):021106–021106, 2010.
- [6] Joseph W Goodman. *Introduction to Fourier optics*. Roberts and Company Publishers, 2005.
- [7] Joseph W Goodman and Randy L Haupt. *Statistical optics*. John Wiley & Sons, 2015.

- [8] Victor Guillemin and Shlomo Sternberg. *Symplectic techniques in physics*. Cambridge University Press, 1990.
- [9] Marc Levoy and Pat Hanrahan. Light field rendering. In *Proceedings of the 23rd annual conference on Computer graphics and interactive techniques*, pages 31–42. ACM, 1996.
- [10] Shree K Nayar. Computational cameras: Redefining the image. *Computer*, (8):30–38, 2006.
- [11] Ren Ng. *Digital light field photography*. PhD thesis, stanford university, 2006.
- [12] Ren Ng, Marc Levoy, Mathieu Brédif, Gene Duval, Mark Horowitz, and Pat Hanrahan. Light field photography with a hand-held plenoptic camera. *Computer Science Technical Report CSTR*, 2(11), 2005.
- [13] Maciej Sypek. Light propagation in the fresnel region. new numerical approach. *Optics communications*, 116(1):43–48, 1995.
- [14] Maciej Sypek. Reply to the comment on “light propagation in the fresnel region–new numerical approach”. *Optics Communications*, 282(6):1074–1077, 2009.
- [15] Emil Wolf. *Introduction to the Theory of Coherence and Polarization of Light*. Cambridge University Press, 2007.
- [16] Kurt Bernardo Wolf. *Geometric optics on phase space*. Springer Science & Business Media, 2004.

- [17] Changyin Zhou and Shree K Nayar. Computational cameras: Convergence of optics and processing. *Image Processing, IEEE Transactions on*, 20(12):3322–3340, 2011.